WATER
WATER
WATER
WATER
WATER
WATER
WATER
WATER
WATER
WATER

Project Completion
Report No. 714438

MECHANISM OF SEMIFLUIDIZED BED BIOREACTOR FOR BIOLOGICAL PHENOL DEGRADATION

Liang-Shih Fan
Department of Chemical Engineering
The Ohio State University

United States
Department of the Interior

Contract No.
A-060-OHIO

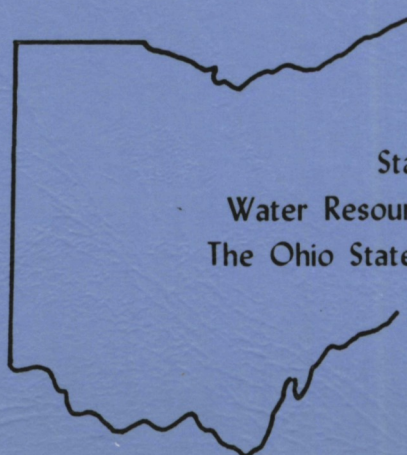

State of Ohio
Water Resources Center
The Ohio State University

Mechanism of Semifluidized Bed Bioreactor for Biological Phenol Degradation

Final Report

OWRT Project No. A-060
(September 1, 1979 - August 31, 1982)

by

Dr. Liang-Shih Fan
Principal Investigator
Department of Chemical Engineering
The Ohio State University
Columbus, Ohio 43210

1983

Table of Contents

Abstract

The kinetics of biological phenol degradation and the performance of the bacteria in a packed bed and semifluidized bed reactor were investigated in this research project. Batch studies at three temperatures, 24°C, 35°C, and 45°C, were undertaken to determine the optimum operating temperature. Sewage bacteria acclimated to high phenol concentrations at each temperature were used in these studies. It was determined that the optimum operating temperature was dependent on the phenol concentration with a rule-of-thumb operating temperature found to be around 35°C.

The bacteria were seeded onto various types of packing material for use in the semifluidized and packed bed studies. In the semifluidized bed, the flow of gas and liquid was countercurrent. From the semifluidized bed studies a decrease in the liquid flowrate from 1500 ml/min to 100 ml/min increased the phenol degradation by approximately 10 percent. From the packed-bed studies an increase of air flowrate from 0 SCFH to 7 SCFH increased the amount of phenol degraded by approximately 4 percent. The bacteria appeared to attach better to the polypropylene packing used in the packed-bed runs than to the charcoal and polyethylene packing used in the semi-fluidized-bed runs.

Investigation was also extended to cover the hydrodynamic behavior of the semifluidized bed. Separate experiments were conducted to study the hydrodynamic behavior of countercurrent flow of gas and liquid in a packed bed. This part of the study simulates the packed section of the semifluidized bed. A mathematical model is developed to account for the friction factor between the liquid and solid in the packed bed. The gas hold-up and friction factor of the packed bed were analyzed and empirically correlated. A computational procedure was developed which allows a reasonably accurate prediction of the pressure drop in the semifluidized bed.

I. INTRODUCTION

1.1 General

The decreasing supplies of natural gas and oil in this country and the growing need for clean fossil fuels has resulted in accelerating the development of coal technology. The United States has 149.6 billion tons of known commercially available reserves of coal and uses approximately 0.339 billions tons per year (refer to Table 1.1). Assuming a commercially available liquefaction or gasification process, over one billion tons of coal per year must be converted to replace the annual shortage of approximately 4.7 billions barrels of oil projected for 1985 (6).

At this time there are only two commercially available units for the production of high BTU gas from coal, the Lurgi and the Koppers-Totzek gasifiers (31). Other processes for coal liquefaction or gasification are either at the pilot plant or bench scale level of development.

The waste liquor streams from coal liquefaction, gasification, or carbonization processes are qualitatively similar in chemical composition. High concentrations of phenolic compounds, thiocyanates, cyanides, sulfides, sulfates, and ammonia are usually found in these wastewaters. Some of the components of the waste stream including ammonia, phenol, and hydrogen sulfide (H_2S) may be present in sufficiently high concentrations to be recoverable. Both ammonia and hydrogen sulfide could be recovered by stripping processes, while phenol recovery could be achieved by solvent extraction. The dephenolated liquors may require further treatment because their phenol levels will probably be greater than 50 mg/L (40). The phenolic compounds are very troublesome water contaminants since toxic polychlorinated phenols can be produced when a water containing phenol is chlorinated.

Table 1.1 - Coal Reserves in the United States and 1970 Production (6)

	Economically Available Reserves, Billion Tons	Recoverable Reserves, Billion Tons	1970 Production, Billion Tons	Life of Recoverable Reserves at 1970 Production Rate, Years
Underground	209.2	104.6	0.339	309
Surface	--	45.0	0.264	170

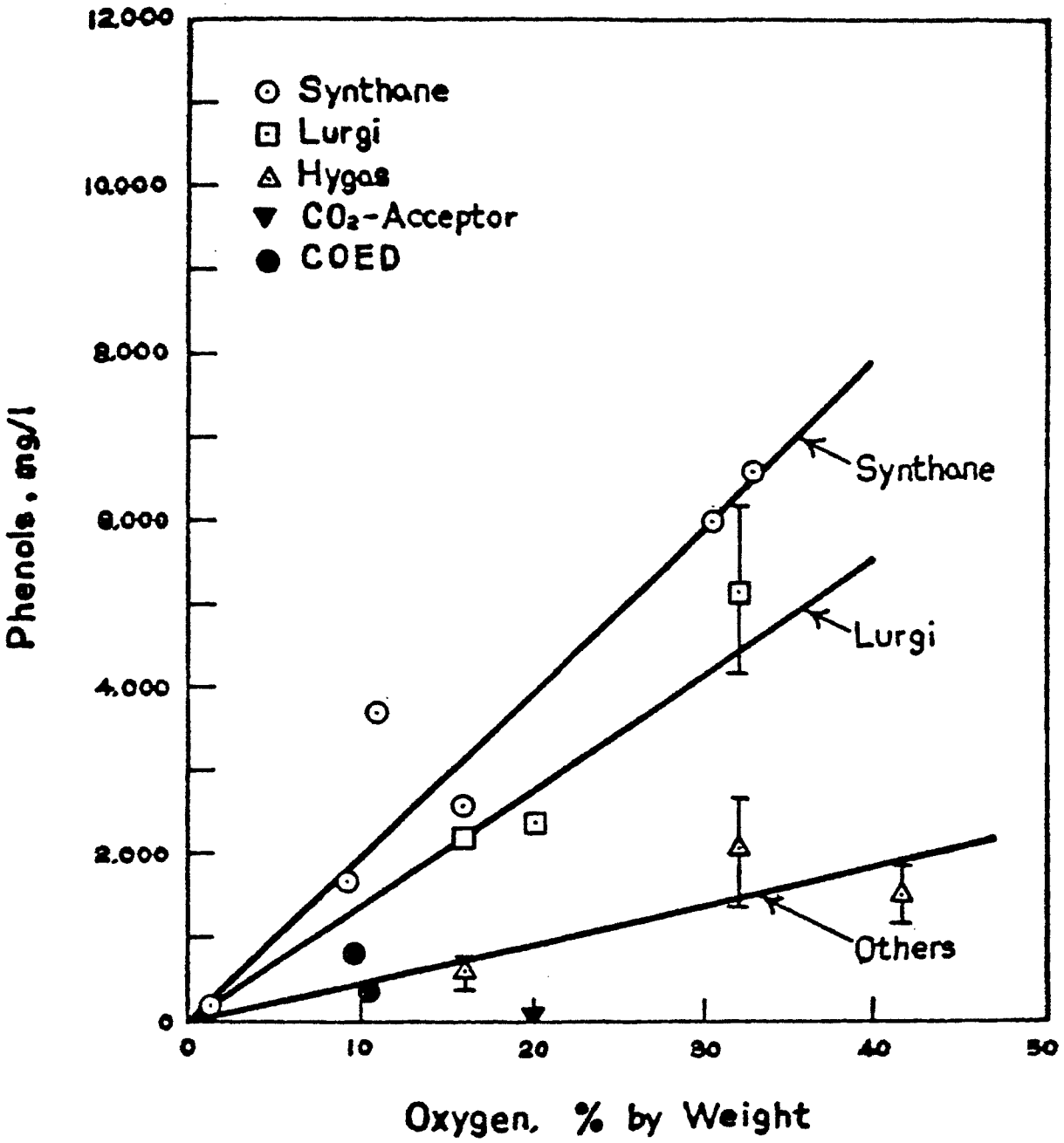

Figure 1.1 Correlation of phenols in effluents with oxygen content in coals (51)

Very little information exists on the quality of the effluents from different synfuel processes for a wide range of coals. Skidmore, et al. (51) developed a correlation technique by which the concentration of the principal types of contaminants produced by the various synfuel processes could be compared to the level of a major constituent of the coal used in that process. Figure 1.1 shows that the concentration of phenol in the effluent from different synfuel processes correlated linearly with the percentage of oxygen found in the coals used in the processes. The oxygen in coal is often bound in some type of phenolic structure. Some of these phenolics are not affected during the gasification or liquefaction of the coal; therefore, they pass unaltered into the product streams and eventually appear in the waste effluents from synfuel operations.

In order to eliminate all polluting compounds in one step, a biological process in which highly evolved symbiotic populations of bacteria (either aerobic or anaerobic) in a reactor configuration may be applied. Although extensive biodegradation facilities for the treatment of coking waste liquors have been operating in the United States for a number of years, the basic reactor design continues to be the simple activated sludge aeration tank followed by a clarifier (32). Extensive research on the treatment of coal waste liquors in a fluidized-bed reactor has been published but very little research into the use of a semifluidized-bed bioreactor for any type of waste treatment has been conducted.

1.2 Objectives of Research

The research work covered in this study was divided into two sections. In Section One of the research, the phenol utilizing bacteria were isolated

from domestic sewage and acclimated to high phenol concentrations. The effect of temperature on the phenol degrading abilities of the diverse microbial population was also investigated. The activity of the bacteria in a semifluidized bed reactor system was then examined. The bacteria were seeded into the reactor system where they attached themselves to the packing and internals of the reactor. Various operating conditions were investigated to determine their effect on the bacterial phenol degradation rate. In Section Two of the research, the hydrodynamic characteristics of semifluidization were explored. Mathematic models were developed to account for the gas holdup, pressure drop and packed bed height in the semifluidized bed.

II. BACKGROUND INFORMATION AND LITERATURE REVIEW

2.1 Bioreactors

Three types of attached growth bioreactor systems, i.e., the packed bed system, the fluidized bed system, and the semifluidized bed system, have been proposed for the microbial treatment of wastewater. The three systems differ mainly in their mode of operation. In the packed bed system, the packing onto which the bacteria are attached stays stationary and is not moved about by the flow of air and wastewater. In contrast, the packing in the fluidized system is in constant movement and the particles are more or less free to move through the bed since they are no longer in continual contact with each other. The semifluidized bed system incorporates both a packed section and a fluidized section of packing in series within the reactor system.

This section will describe the three reactor systems in greater detail. The advantages and disadvantages of the reactor systems will be compared and contrasted.

Packed Bed Bioreactors

Several wastewater treatment applications have been proposed for packed-bed reactors (PBR). Effective anaerobic treatment of concentrated soluble wastes in an upflow submerged "anaerobic filter" was reported by Young and McCarty (63) in 1969. Successful anaerobic denitrification in PBR units was demonstrated by Haug and McCarty (26) and Requa and Schroeder (49). An Aerobic sand-medium "pulsed absorption bed" process for providing additional treatment of low quality effluents from secondary wastewater treatment plants was described by Johnson and Baumann (35). Young, et al. (62) reported both

secondary effluent biochemical oxygen demand (BOD) removal and ammonia removal in packed-bed reactors. Phosphorus transport in packed-bed reactors was reported by Overman, et al. (45). Phenol degradation using an aerobic PBR was reported by Holladay, et al. (32).

The basic packed-bed reactor designs used for the preceding applications were essentially similar. The reactor consisted of a container (reactor) which was packed with a medium to which bacteria could become attached. Influent wastewater was introduced through the reactor bottom by use of an underdrain system or inlet chamber. In aerobic units, either air or oxygen enriched air was introduced into the system from an air distribution grid located immediately below or slightly above the bottom of the media bed. The media selection depended primarily on the particular application of the PBR system. Some of the commonly used packing media were sand, coal, plastic packings, and activated carbon.-

According to Young et al. (62) the three principal mechanisms by which the removal of organic material is accomplished in PBR's are:

1. Colloidal and soluble organic wastes are converted to backterial cells that may be separated from the wastewater.
2. The total mass of settleable and unsettleable cells is reduced through endogenous respiration.
3. Specific soluble wastes are adsorbed on the PBR media surface where they become availalle to the attached bacteria.

It is a combination of the three mechanisms, i.e., adsorption, respiration, and synthesis that remove organic material from wastewater. Therefore, the total organic material removed by the PBR unit will be the sume of:

1. Organic material converted for biological growth and metabolism;

2. Bacterial cell solids reduced through endogenous respiration; and

3. Suspended solids removed by filtration or other mechanical means.

The PBR effluent will contain primarily nonbiodegradable organic and soluble inorganic wastes.

Several models have been developed for various PBR systems. Requa and Schroeder (49) have shown that a homogeneous model composed of a series of stirred-tank reactors provided a satisfactory description of a packed-bed denitrification reactor. Overman, et al. (46) developed a model for phosphorous transport in a packed-bed reactor in which convection, adsorption, desorption, and chemical reaction were all included in the adsorbed state.

Fluidized Bed Bioreactor

Fluidization is used to achieve an intimate, uniform contact between a fluid and solid particles. As the velocity of a fluid passing up through a bed of particles is increased, a point is reached at which the upward force is sufficient to lift the particles and expand the bed. The individual particles are more or less free to move through the bed since they are no longer in continual contact with each other. As the fluid velocity is further increased, the void fraction increases toward unity and the particles eventually become sufficiently separated so that they behave as single particles. If the upward force on a particle becomes significantly greater than its weight, it is swept completely out of the bed. Thus, fluidization resembles flow through a packed bed at the minimum fluidization velocity and flow past a single particle at high velocity (4).

Several wastewater treatment applications of the fluidized-bed bioreactor (FBBR) have been reported. Holladay et al. (32) reported high phenol degradation rates using a synthetic phenolic feed, while Lee et al. (40) reported phenolic and, to a lesser extent, ammonia degradation in a tapered FBBR unit. Jeris, et al. (34) demonstrated that anaerobic denitrification of wastewater can be successfully accomplished using a bench scale fluidized-bed with sand as the fluidizing media. Jeris and Owens (33) reported successful operation of a pilot-scale denitrification FBBR unit. A commercial FBBR (manufactured and marked by Dor-Oliver, Inc. of Stanford, Conn.) is currently available (57).

The FBBR can be designed with either a tapered or cylindrical vertical reactor bed. The tapered fluidized bed resembles a truncated cone in which there is a gradual expansion from a relatively small entrance cross sectional area to an exit cross sectional area which may be several times larger than the entry. If the entry cross section is sufficiently small and the expansion is gradual (an angle of a few degrees), the flow should be relatively stable throughout the reactor. There should also be few large eddies thus providing flow patterns that have minimal backmixing, especially at the feed entry point. The tapered FBBR can effectively operate over a wide range of feed flow rates without loss of bed material since the fluid velocity decreases with reactor height. Unlike a FBBR with a constant cross-sectional area, at higher flow rates the tapered bed simply expands into a portion of the reactor having a larger cross-sectional area. Therefore, at very high flow rates, the lower portion of the reactor may be relatively free of the fluidized packing material, since the fluid velocity may greatly exceed the settling velocity of the particles at that point. At the same time, a lower

fluid velocity further up the reactor may result in the bed being only slightly above incipient fluidization, thus preventing loss of the fluidized particles (49).

In contrast, the constant cross-sectional area FBBR is simply a cylindrical vertical column filled with a fluidizing medium. The wastewater is introduced at the bottom of the column through a distribution place.

Several mathematical models have been proposed to describe the fluidized bed bioreactor. Scott and Hacher (49) developed an empirical mathematical model predicting bed expansion, pressure drop, and chemical reactivity in a tapered FBBR. Their model was developed by considering the reactor to be a series of discrete cylindrical sections with each subsequent section having a larger diameter. Pitt et al. (48) developed a differential model based on the continuity equation and simple chemical kinetics. The concentration profile and the reaction rate coefficient has been solved for both first order and nth order steady state plug flow reactions in a tapered fluidized bed reactor. Weber and Ying (58) developed models for expanded (or partially fluidized) cylindrical beds of both biologically and nonbiologically activated carbon.

Semifluidized Bed Rdactor

The phenomenon of semifluidization was first reported in 1959 by Fan et al. (21). The semifluidized bed incorporates the features of both the fixed and fluidized beds by partially restricting expansion of the fluidized bed. A semifluidized bed is formed when a mass of fluidized particles is compressed with a porous restraining grid. This gives rise to the creation of a fluidized bed and a fixed bed in series within a single containing

vessel. The internal structure of a semifluidized bed can be easily altered to continuously create an optimal operating configuration. This unique feature allows the use of the semifluidized bed for a wide range of industrial and practical applications as greater emphasis is placed on the design and maintenance of an efficient process plant. Fundamental information on the semifluidized bed has been limited to only the two phase systems, i.e., gas-solid and liquid-solid systems. There is no fundamental information available concerning the semifluidized bed operation in the three or more phase system.

Several industrial applications of the semifluidized bed reactor have been proposed. Asahi Chemical Company of Japan (8) and Bayer AG of Germany (9) are promoting the use of semifluidized beds with ion exchange resins. This development resulted from the discovery that a fluidized bed, followed by a fixed bed, increases the efficiency of resin utilization by improving liquid-resin contact. The fixed bed acts as a polishing section, handles the ion leakage from the fluidized bed, and prevents elutriation of resin particles. In addition to a higher resin utilization efficiency, semifluidization also minimizes the volume of regenerant and wash water needed, reduces pressure drop, and operates more consistently than the conventional fixed bed process. Another semifluidized bed reactor application, the adiabatic oxidation of benzene, was reported by Babu Rao et al. (1).

Fan et al. (20) (21) investigated the rate of mass transfer in a semifluidized bed system composed of benzoic acid spheres and water. They found that the depth of the packed section, and consequently the fluidized seciton, was a function of flow conditions, particle and fluid characteristics, and the expansion of the bed allowed. The rate of mass transfer was also affected not only by the characteristics of the particles, fluids, and

flow rate but also by the amount of expansion of the bed. By means of bed expansion alone, the magnitude of the semifluidized mass transfer coefficient was able to be varied approximately linearly between the mass transfer coefficients for fluidized and fixed bed systems. The experimentally determined log-mean mass-transfer coefficients, k_{lm}, in a semifluidized bed was therefore given by $(1-X)(k_f)_{lm} + X(k_{pa})_{lm}$ where k_{lm} is the log mean mass-transfer coefficient, $(K_f)_{lm}$ is the log mean mass-transfer coefficient of the fluidized section in the semifluidized bed, $(k_{pa})_{lm}$ is the log mean mass-transfer coefficient of the packed section in the semifluidized bed, and X is the weight fraction of particles in the packed section of a semifluidized bed. It was also determined that the pressure drop through a semifluidized bed was the sum of the pressure drops through the fluidized and packed portions of the bed.

Fan and Wen (20) also studied packed bed formation and pressure drop increase when semifluidized beds were formed by the compression of fluidized bed. Methods for obtaining the minimum semifluidization velocity, i.e., the velocity at which the formation of the packed portion initiates, and the maximum semifluidization velocity, i.e., defined as the fluid velocity at which all solid particles are supported by the fluid in the packed portion of the bed, in solid-liquid systems were also proposed. Wen, et al. (60) extended the study of semifluidization to solid-gas systems and found the results very similar to the liquid-solid systems investigated earlier.

Comparison of the Biological Wastewater Treatment Methods

Holladay, et al. (32) compared phenol degradation in stirred-tank, packed-bed, and fluidized-bed reactors. Although the highest phenol

concentrations in the influent could be treated in the stirred-tank reactor, this treatment method required the largest reactor volume and longest retention time. The largest degradation rates and lowest retention times along with the greatest resistance to system fluctuations were observed for the packed- and fluidized-bed bioreactors. It was concluded that the efficiency for degrading phenolic liquid among the three types of bioreactors increased in the following order: stirred-tank bioreactor, packed-bed bioreactor, fluidized-bed bioreactor. The degradation rates were found to be dependent upon the state of biomass development, air flow rate, liquid flow rate, and feed concentration.

The high efficiency of the fluidized-bed bioreactor may be attributed to the concentration of active biomass within the reactor. The small media particles in the column give the bacteria a very large surface area on which to grow. As a result, the average concentration of bacteria (measured as total volatile solids) in the reactor is between 30,000 and 40,000 mg/L. This high concentration of biomass, which is 10 to 20 times greater than that in conventional systems, allows the effective time for treatment to be reduced from hours to minutes with a corresponding savings in system space requirements (33).

The main advantages of the stirred-tank reactor are the simplicity of operation and the ease with which its retention time may be adjusted. The main disadvantages of the stirred tank reactors are its vulnerability to shocks, its slow recovery time from fluctuations, and its vulnerability to washout (32).

The chief advantages of the packed-bed bioreactor are twofold: the active bacteria are held on a stationary surface; and the bed recovers

quickly from shocks. The main disadvantage of the packed-bed bioreactor is its inherent tendency to develop excess biomass, which results in both a high pressure drop across the bed and severe flow stoppages. Both problems are not easily rectified in a continuous operation (32).

The fluidized bed bioreactor has the following advantages: utilization of a small particulate packing that allows for bacterial coating of a large surface area; use of a packing material that may be easily regenerated or replaced as a continuous operation; application of a bed with low pressure drop characteristics; simple utilization of air or air/oxygen mixtures when aerobic bacteria are the active organisms; no danger of clogging due to excessive bacterial growth; treatment of greater volumes of waste per unit time since greater flow rates may be used with insignificant head losses (32), (34).

Large economic savings can also be realized with a fluidized bed system. The large concrete tanks or basins necessary with conventional stirred-tank wastewater treatment systems are replaced by compact reactors containing a bacteria saturated medium having a high biomass concentration. Ecolotrol, Incorporated, the developer of the commercial fluidized bed bioreactor states that the fluidized bed system can save 20 to 30 percent of the capital costs of a conventional system and about 60 percent of the conventional construction time. Operating costs of a fluidized bed system are comparable to those of standard methods of waste treatment. Since the fluidized bed system operates with a captive population of active biomass, there is no requirement of returning activated sludge to the reactor. This eliminates the need for a clarification step after after the reactor. An

added benefit is that expansion of an existing plant may be accomplished simply by adding fluidized bed bioreactor units, and, if the treatment plant is needed elsewhere, the modules can be transported by rail or truck (57).

The disadvantages of the fluidized bed bioreactor are as follows: difficulty in obtaining good liquid-solid disengagement; poor degradation of any compound requiring long retention time; narrow range of liquid flow rates over which there is stable operation; difficulty in maintaining non-fluctuating operation at desired conditions since high bed expansion and low stability can occur frequently; attaining and maintaining even flow distribution throughout the reactor cross section, especially close to the feed entry point (32), (40), (50).

Another major problem with the fluidized-bed bioreactor system is the need to control the biological growth on the fluidized particles. The bed expansion increases as the particle weight increases due to bacteria growth. As expansion continues, it may eventually become necessary to remove a portion of the biologically coated media to prevent bed overflow. It has been found that periodic backwashing of the bed helps remove a portion of the excess biological growth (34).

The semifluidized bed bioreactor would eliminate some of the difficulties encountered with the fluidized bed bioreactor, such as elutriation of the particles coated with microorganisms and unstable bed expansion. Since the fluidized portion of the bed will carry the main load of digestion with the packed portion acting as a polishing section, the fluid reaching the packed section will be lean in bacterial nutrients and thus will not excessively contribute to increases in cell masses that can clog the bed. If the packed section of the bed becomes plugged by excess cells or by suspended

solids, the clogging can be cleared by raising the upper porous septum and completely fluidizing the bed. To control the microbial population, the entire bed should periodically be fully fluidized during which the excess cell mass is sheared from the fluidizing particles. A savings of a but 95 percent in space can be realized by installing a simifluidized bed bioreactor instead of a conventional suspended growth waste treatment unit (19).

Another advantage of a semifluidized bed bioreactor is its capability to self-regulate the flow rate. As the flow rate of influent wastewater is increased (decreased) either accidentally or cyclically, the height of the packed portion is also increased (decreased), thus resulting in a higher (lower) pressure drop, which, in turn, reduces (increases) the flowrate. This naturally gives rise to a stable, self-regulatory system. Such a system is desirable in wastewater treatment because of the flow rate of municipal or industrial wastewater varies erratically and diurnally (19).

Table 2.1 summarizes the efficiency of the various wastewater treatment systems on the market today.

2.2 Metabolic Pathways for the Biological Degradation of Phenol

The utilization of aromatic compounds by certain bacteria has been observed by many investigators. Happold (25) observed the capacity of bacterial suspensions to oxidize many aromatic compounds including phenol. Evans (16) isolated phenol utilizing organisms from the faeces of several mammals, i.e., cow, horse, sheep, pig, and man, and these bacteria appear to be normal inhabitants of the intestine.

Two metabolic pathways for the microbial degradation of phenol exist. In the ortho-fission pathway, catechol (the first metabolite of phenol) is split between the adjacent hydroxyl groups with succinate and acetate being the final degradation products. In the meta-fission pathway, catechol is

Table 2.1 - Efficiencies of Commercially Available Wastewater Treatment Methods (reported in lb BOD removed per 1000 ft^3 of reactor volume/d) (57)

Hy-Flo Fluidized-Bed System	1000
Pure-Oxygen-Aeration System	200
Suspended-Growth System	50
Rotating-Disk System	50
Trickling-Filter System	25

split on either side of the two adjacent hydroxyl groups with the final degradation products being formate, acetaldehyde, and pyruvate. Both pathways will be described in the following sections.

Ortho-Fission Pathway

Evans (16) suggested the following pathway for the degradation of Phenol:

> Phenol → catechol → o-benzoquinone → possibly further oxidized ring componds → ketonic and aldehydro-acids (by ring fission) → formic acid and other compounds

O-benzoquinone was shown to be produced by the isolation of a di-anilino derivative; formic acid was isolated from a bacterial culture in which phenol had disappeared; and a transient inetermediate compound indicative of a keto-acid was observed. Kilby (37) identified the keto-acid as 2-ketoadipic acid and suggested the following pathway:

> phenol → catechol → o-benzoquinone → 1, 2, 5-trihydroxybenzene → 5-hydroxy-o-benzoquinone → 2-ketoadipic acid → succinate and acetate

Stanier et al. (53) considered 1,2,5-trihydroxybenzene a highly improbable intermediate compound since its degradation was nonenzymatic and the Rothera reaction was completely negative at the end of the oxidation. The following metabolic pathway was therefore suggested:

> phenol → catechol → o-benzoquinone → muconic acid → 2-hydroxyadipic acid → 2-ketoadipic acid

1,2,5-trihydroxybenzene was nc longer considered an intermediate compound. This implied that catechol could not be further oxidized without loss of aromatic character since 1,2,5-trihydroxybenzene was the only trihydroxybenzene in which the positional relationships of the oxidized and reduced carbon atoms were such that a subsequent opening of the ring

between any two carbon atoms could give rise to the positional relationships of oxidized and reduced carbon atoms that exist in the molecule of 2-ketoadipic acid.

Kilby (38) observed the C_4-C_2 split of 2-ketoadipic acid to succinate and acetate and thus the final step before the entry of phenol into the terminal respiratory cycle was determined.

The intermediates between catechol and 2-ketoadipic acid were now to be determined. Hayaishi and Hashimoto (28) isolated and purified an enzyme system which they termed pyrocatecase. This enzyme was able to convert catechol to what Hayaishi and Hashimoto believed to be cis-cis-muconic acid. When the cis-cis-muconic acid was later isolated and tested with a known enzyme system that catalysed the degradation of catechol to 2-ketoadipic acid, no 2-ketoadipic acid was formed and therefore it was believed that cis-cis-muconic acid could not be a true intermediate (17). At this same time Elvidge et al. (15) were investigating the stereochemistry of the muconic acids. Cis-trans-muconic acid was isolated and found to very closely resemble cis-cis-muconic acid, i.e., the melting points of the free acids were nearly the same and their dimethyl esters had almost identical melting points. It was also discovered that when cis-cis-muconic acid was boiled with water (as is done in the usual processes of purification), the acid was inverted to the cis-trans-isomer.

Evans and Smith (18) examined the acids as substrates in the biodegradation of catechol. They determined that bacterial enzymes do convert catechol to 2-ketoadipic acid through the formation of cis-cis-muconic acid. All other isomers of muconic acid were found to be enzymatically inactive. Therefore in the process of isolation and purification of cis-cis-muconic

acid by Hayaishi and Hashimoto isomerification to the cis-trans form must have accrued and therefore the negative results. Evans and Smith suggested the degradation pathway for phenol as follows:

Phenol → catechol → o-benzoquinone → cis-cis-muconic acid → 2-ketoadipic acid → simpler organic acids

Evans et al. (17) proposed the following reaction sequence (see Figure 2.1) since -carboxymethyl-Δα-butenolide had been synthesized:

catechol → cis-cis-muconic acid → -carboxymethyl-Δα-butenolid → 2-oxoadipate enol-lactone (hypothesized at this time) → 2-ketoadipic acid

Hayaishi, et al. (29) suggested the following intermediate (1) in the biodegradation reaction of catechol to cis-cis-muconic acid due to work they had done with O^{18}:

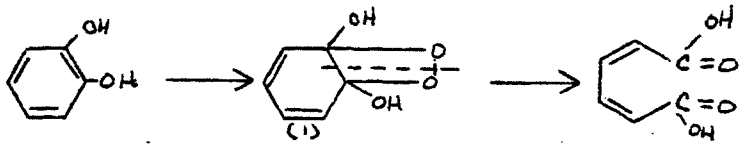

It was also felt that o-benzoquinone was unlikely to be an intermediate since H_2O_2 was shown not to participate in the reaction unless it was so tightly bound to an enzyme acting as a peroxidase as to be chemically undeterminable.

Ornston and Stanier (44) proved 2-oxoadipate enollactone to be in the metobolic pathway between -carboxymethyl-Δα-butenolide and 2-ketoadipic acid.

Meta-Fission Pathway

The pathway for the meta-fission degradation of catechol is known in less complete detail than the ortho-fission pathway. The oxidation of catechol by meta-fission was first reported by Dagley and Stopher

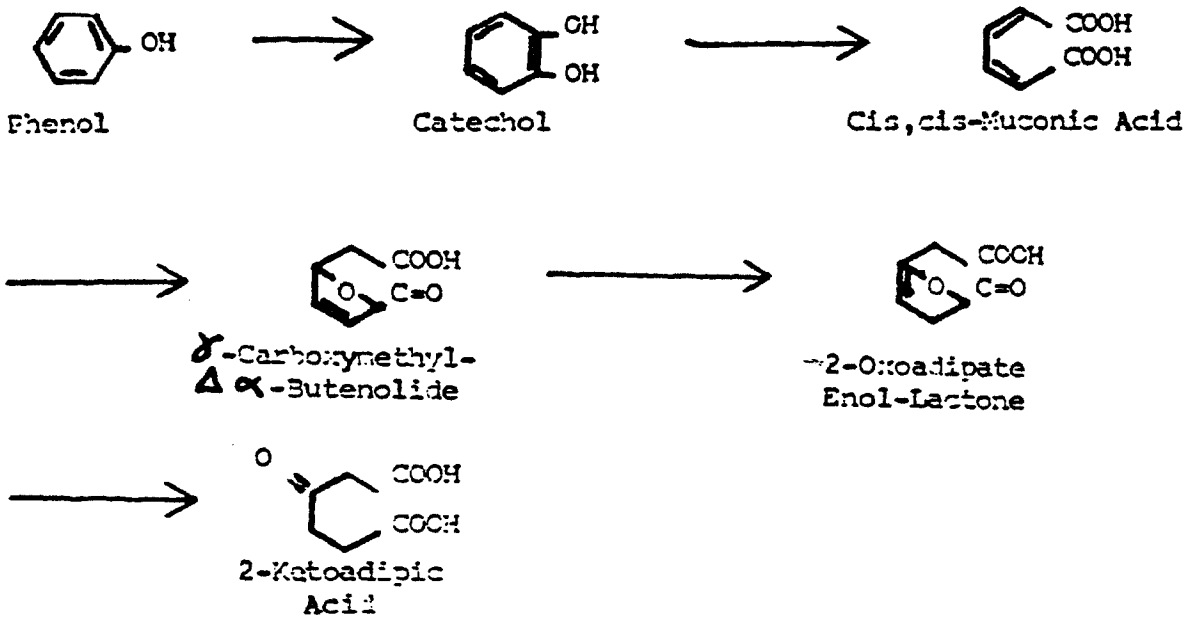

Figure 2.1 Ortho-Fission Pathway as Proposed by Evans, et.al. (9)

(13). The degradation pathway tentatively suggested was:

catechol → 2-hydroxymuconic semialdehyde → 2,4-dihydroxy-muconic semialdehyde → malondialdehyde + pyruvate → 3-hydroxypropionic acid

Conversion of the keto to enol form of 2-hydroxymuconic semialdehyde was suggested by Dagley et al. (11) with the subsequent degradation of the keto form of 2-hydroxymuconic acid to the pyruvate and other products.

Nishizuka (42) showed the product of ring fission to be 2-hydroxymuconic semialdehyde and that acetate and pyruvate were formed by a reaction sequence that involved two oxidative steps and a decarboxylation of 4-oxalocrotonate. The following pathway was proposed:

catechol → 2-hydroxymuconic semialdehyde → carbon dioxide + 4-oxalocrotonate → 4-hydroxy-2-oxovalerate 2,4-dioxovaleric acid → acetate + pyruvate

Dagely et al (12) confirmed the observations of Dagley and Stopher and also showed that 2-hydroxymuconic semialdehyde was metabolized to formate, acetaldehyde, and pyruvate by the proposed pathway:

catechol → 2-hydroxymuconic semialdehyde → 4-hydroxy-2-oxovalerate → formate + acetaldehyde + pyruvate

4-oxalocrotonate was not an intermediate in the proposed reaction sequence but could possibly be a metabolite of the Pseudomonas used by Nishizuka.

Bagly et al. (3) proposed two possible pathways for the conversion of 2-hydroxymuconic semialdehyde to 4-hydroxy-2-oxovalerate (see Figure 2.2) Bagly and Dagley (2) found 2-oxopent-4-enoate to be the intermediate compound in the conversion of 2-hydroxymuconic semialdehyde to 4-hydroxy-2-oxovalerate (pathway B in Figure 2.2)

2.3 The Phenol Degrading Bacteria

The ability to utilize aromatic substances is not universal among

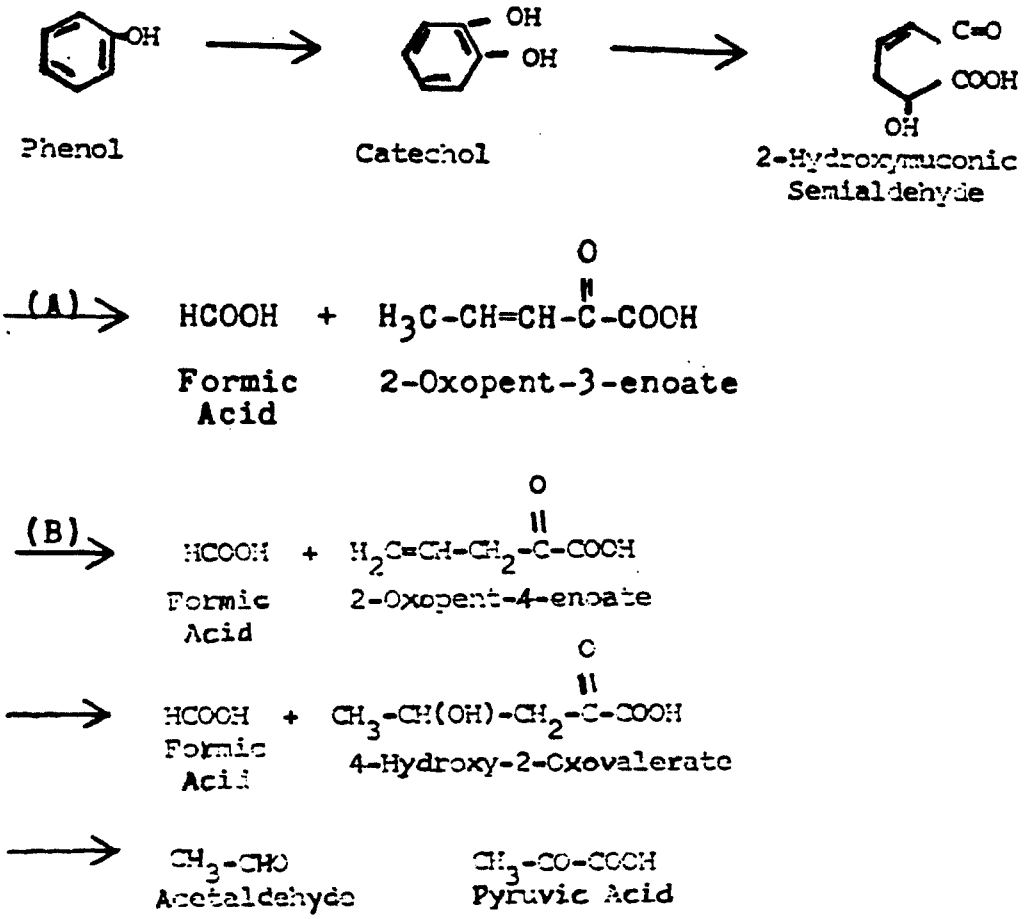

Figure 2.2 Meta-Fission Pathway as Proposed by Bayly, et.al. (3)

bacteria. Low concentrations of phenol and phenol derivatives can cause the eventual death of bacterial cells resulting from the inactivation of essential enzyme systems.

Callely (7) suggests that bacteria have had to acquire the ability to degrade the aromatic chemicals by developing new metabolic sequences to feed such compounds into their existing central metabolic pathways. The degradation ability could be acquired by:

1. a change in the specificty of the enzymes which already possess a little activity towards the new compounds;
2. the production of an already inducible enzyme;
3. a decreased sensitivity to the new compounds and any of the metabolites which may have been toxic; and
4. the increased permeability of the organism to the new compounds.

Numerous researchers have isolated microorganisms capable of metabolizing phenol and phenolic substances. Evans (17) listed the following bacteria families as having this metabolic ability: Coccacae, Mycobacteriaciae, Bacteriacea, Pseudomonadaceae, Spirallaceae, and Bacillaceae. Holladay et al. (32) found the following bacteria present when biologically treating coal waste liquors: Bacillus, Staphylococcus (not aureus), Pseudomonas, Citrobacter, Proteus, and Escherichia coli.

Table 2.2 lists some of the bacteria capable of degrading phenol. The growth characteristics are listed as found in Bergey's Manual of Determinative Bacteriology (5) with the exception of P. phenolis whose growth characteristics are given by Weiser et al. (59).

Table 2.2 - Physical Characteristics of Phenol Utilizing Organisms*

Organism	Temperature Range	ph Range	Habitat	Other Utilizable Compounds
Bacillus closteroides	13-30		water, soil, feces, decaying vegetables	
Flavabacterium helulolum	25-37		water, soil	
Pseudomonas				
P. cruciviae	30-35		soil	m-cresol
P. dacunhae	25		soil	
P. desmolyticum	25		soil	napthelene
P. fluorescens	20-25		soil, water	
P. phenolis	37-54	6.5-7.5	sewage	m-cresol
P. putida	25-37		water, putrefying materials	
P. rathonis	25		manure, soil	cresol, napthelene

*P. phenolis from Weiser, et al. (59); all others from Breed, et al. (5).

III. EXPERIMENTALS

A. Biological Study

This section describes the equipment and experimental procedure used in both the acclimation of the phenol bacteria (Phase One) and the semi-fluidized bed and packed bed application (Phase Two) research.

3.1a Bacteria Description and Acclimation Procedure

The mixed bacterial culture used in this study was originally derived from raw domestic sewage obtained from the Water Resources Building on The Ohio State University campus. Raw sewage was chosen for this bacterial study since many of the bacteria capable of degrading phenol are indigenous to water, soil, and fecal material. Evans (16) isolated phenol utilizing organisms from the faeces of several mammals, i.e., cow, horse, sheep, pig, and man, and these bacteria appear to be normal inhabitants of the intestine.

The raw sewage was first diluted 1:1 with a feed solution containing phenol and other elements necessary for microbial growth (see Table 3.1). The phenol concentration was gradually increased from 20 mg/L to 100 mg/L over a three-week period. Sucrose was added to the solutions during the first week of acclimation but was discontinued after that time. During Phase One, approximately 10 percent of the stock bacterial solution was wasted three times a week and replaced with freshly made feed solution.

After the completion of Phase One, a bacterial suspension was frozen in order to preserve the acclimated culture for Phase Two of this project. The culture appeared to retain its phenol degrading ability. During Phase Two work approximately 50 percent of the culture was wasted every day and replaced with fresh feed solution. The increase in wasting was due to the

Table 3.1 - Composition of Synthetic Feed

1 liter of tap water (allowed to set for 24 hours in order to dechlorinate)
1 gram of ammonium nitrate
0.2 ml of 85 percent phosphoric acid
phenol (variable)
sucrose (optional, initially during first two weeks of bacterial acclimation, omitted from feed after that period)
0.2 gram of ammonium chloride
pH adjusted to 7.0 with concentrated ammonium hydroxide

* adapted from Holladay, et al. (32)

information obtained from Phase One work, i.e., the bacteria grow so quickly that an increased wasting of the bacteria was necessary in order to keep an actively growing culture. If the feed solution was not replaced daily, the bacteria would consume each other or die off once the phenol was consumed.

During Phase One work, a bacterial population was acclimated at 24°C, 35°C, and 45°C. The three cultures were identically fed and aerated in order to facilitate comparison. Due to the results of Phase One work, only the 35°C culture was frozen and used in Phase Two studies.

The bacterial suspension used in this study was sent to a bacteriology laboratory for identification of the phenol degrading microbes. A detailed copy of the laboratory results can be found in Appendix A. The following phenol degrading bacteria were found in the bacterial culture used in this study: Pseudomonas putida, Providencae alcalifaciens, Citrobacter freundiae, Proteus (Proteus mirabilis possibly), and Flavobacter (this family was not well enough known to determine the specific phenol degrading species present in the culture).

3.2a Analytic Methods

The parameters examined in this study were chemical oxygen demand (COD), phenol, dissolved oxygen (DO), and pH. The pH measurements were made on a Leeds and Northrup pH meter using a Corning electrode. A Yellow Springs Instrument (YSI) oxygen meter and probe were used for all dissolved oxygen measurements.

The phenol and COD samples were preserved since immediate analysis was not possible. The phenol samples were stored in glass bottles before steam distillation and plastic bottles after steam distillation. The phenol

samples were preserved with copper sulfate (5 ml of 100 g $CuSO_4$/1 L distilled water per 500 ml sample) and enough phosphoric acid to reduce the sampel pH to below 4.0. The COD samples were stored in plastic bottles with enough sulfuric acid added to the sample to reduce the pH to below 2.0.

The phenol and COD analysis were performed according to the methods outlined in Standard Methods for the Examination of Water and Wastewater, Thirteenth Edition (52). The phenol samples were first steam distilled and then color developed using aminoantipyrine and potassium ferricyanide. The chloroform extraction method was not used since the samples were in the parts-per-million (ppm) range. After a fifteen-minute color development period, the absorbance was measured using a Bausch and Lomb Spectrophotometer 20 for Phase One and a Bausch and Lomb Spectrophotometer 88 for Phase Two work. The phenol concentration was then determined from a standard curve consisting of known phenol concentrations versus absorbance (see Appendix B for this curve). A phenol standard of known concentration (usually 0.2 mg) was color developed with each set of samples in order to insure accurate analysis.

The titration method using ferrous ammonium sulfate was used for the COD analysis. The water sample was initially mixed with sulfuric acid, potassium dichromate, mercuric sulfate, and silver sulfate. The solution was then refluxed for two hours. The cooled sample was titrated with ferrous ammonium sulfate (using ferroin indicator) and compared against a blank.

3.3.a Experimental Procedure and Equipment for Phase One

Three waterbaths set at 24°C, 35°C, and 45°C were used in this section

of the research. The waterbath temperatures were automatically controlled to ±1°C. The first set of runs was to determine if there was a decrease in phenol concentration due to aeration. At each temperature level a control solution and a bacterial solution (using the appropriate acclimated culture) were run. Initially each bacterial solution consisted of 100 ml of the acclimated culture added to three liters of feed solution containing a phenol concentration of approximately 200 mg/L. The control solution consisted of 100 ml of distilled water added to three liters of feed solution containing a phenol concentration of approximately 200 mg/L. The solutions were sampled periodically and analyzed for phenol and COD by the procedures outlined in the previous section. Each run was terminated when the phenol concentration of the bacterial solutions became less than 1 mg/L.

A second set of experimental runs were then undertaken to determine the effect of phenol concentration on the microbial degradation rate. Phenol concentrations of approximately 450 mg/L and 650 mg/L were used. The bacterial solutions were prepared using 100 ml of the respective acclimated bacterial suspension to three liters of feed. A control was not considered necessary since the first set of experimental runs determined that the loss of phenol was due to bacterial action and not due to other losses.

Throughout the runs, the solutions were continually aerated. Samll plastic balls were floated both in the beakers containing the solutions and the waterbaths to reduce evaporation.

3.4.a Description of Experimental Equipment for Phase Two

The total reactor vessel was composed of five plexiglas sections. These sections were (starting from the top of the reactor) the gas outlet section, the upper distributor plate (for liquid distribution,) the main

reactor column, the lower distribution plate (for air distribution), and the liquid outlet section.

A schematic diagram of the assembled reactor is shown in Figure 3.1. Detailed diagrams of the unique upper and lower distributor plates are shown in Figure 3.2 and Figure 3.3, respectively.

Twelve pressure taps were included in the reactor vessel. Eleven of these taps were located at three inch intervals on the main reactor column and one tap was located on the lower distribution plate. Pressure data was not collected in this study but the taps were used to obtain liquid samples at various points in the reactor.

A lower retaining screen made of hardware cloth with a hole size of approximately 1/8-inch was installed at the bottom of the main reactor column in order to help the reactor drain better by keeping the packing above the liquid outlet tubes.

The upper retaining grid was composed of a stainless steel screen with a hole size of approximately 1/8-inch. A steel ring was brazed around the outside of the screen to keep the screen from fraying and to provide more support. The diameter of each retaining screen was approximately 2-1/4 inches.

A steel rod was attached to the upper retaining grid in order to easily adjust the height of the bed. The rod extended up through the center tube of the upper distributor plate and was held in place by a brass male connector on the upper plate of the gas outlet section.

The sections were bolted together with four 1-1/2 inch carriage bolts. Square gaskets made of 1/16 inch thick rubber sheeting were positioned between the sections in order to make the reactor water tight.

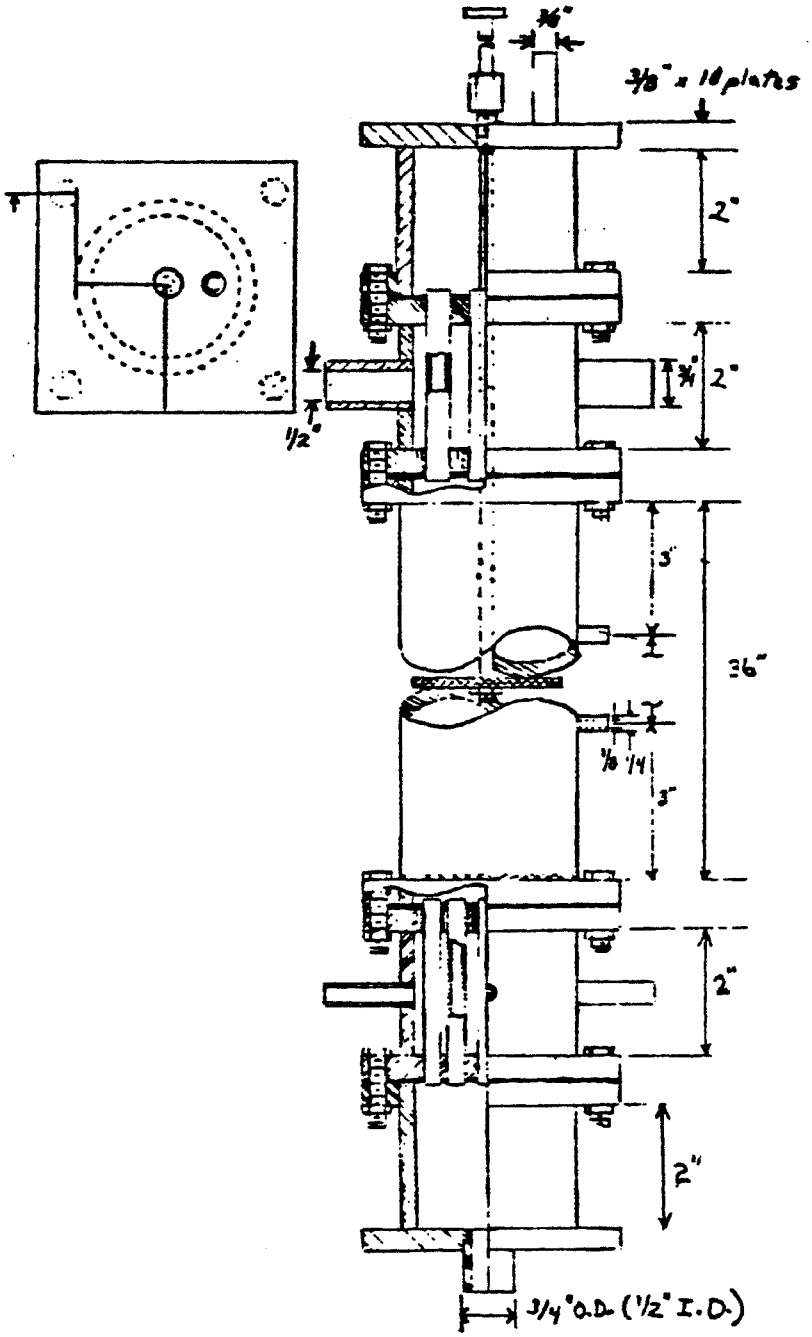

Figure 3.1 Schematic diagram of the assembled reactor

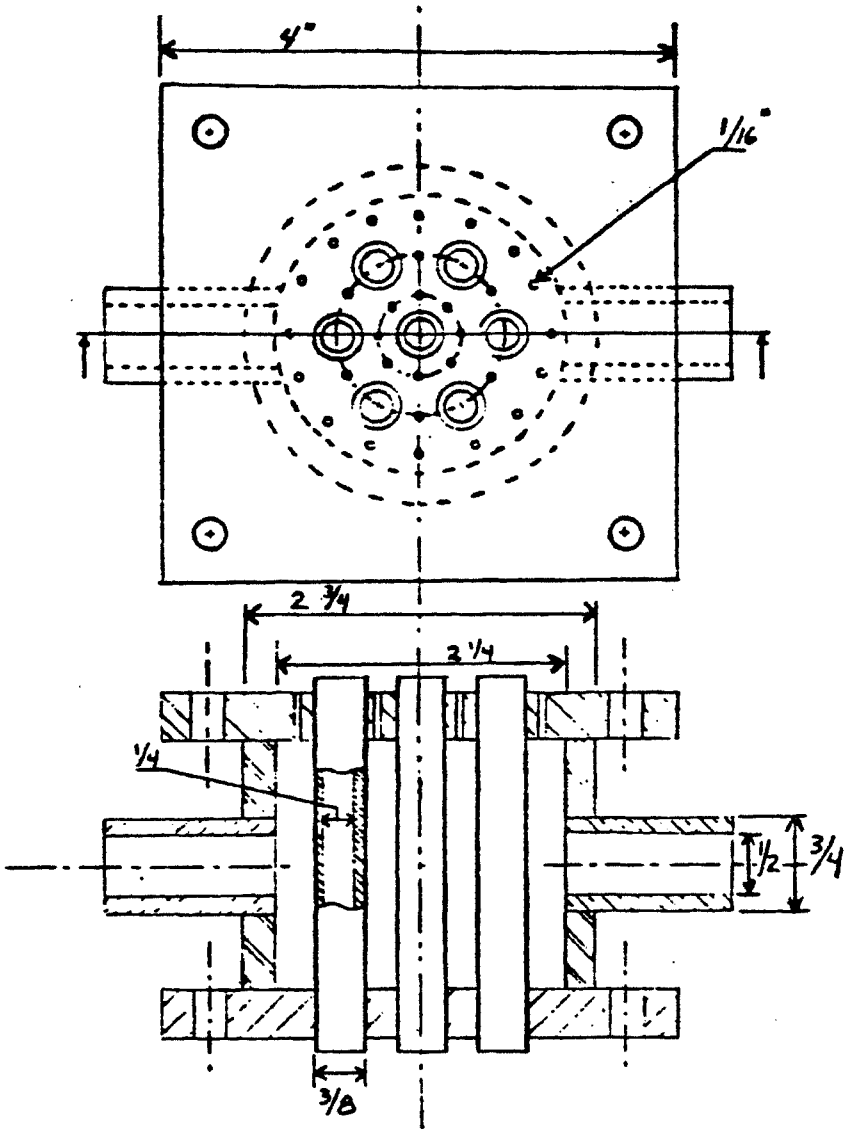

Figure 3.2 Schematic diagram of upper distributor plate

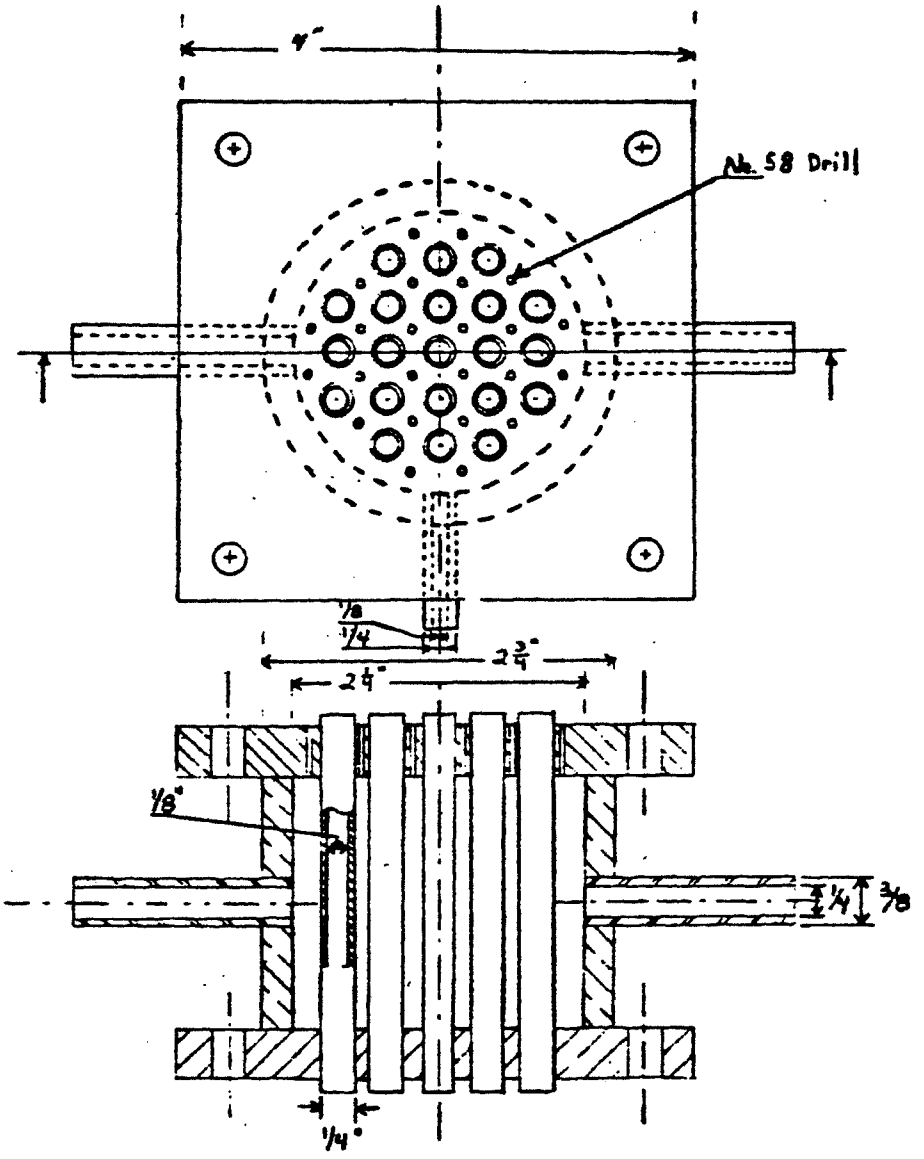

Figure 3.3 Schematic diagram of lower distributor plate

The flowsheet for the total reactor system is shown in Figure 3.4. Each feed tank had a capacity of approximately thirty-two gallons. The heating elements were controlled with Glas-Col variable regulators. A Little Giant pump was used as the feed pump. The liquid rotameter was manufactured by Precision and had a range of 100 ml/min to 2100 ml/min. The air rotameters were manufactured by Dwyer and had a range of 1 SCFH to 10 SCFH and 1 SCFH to 100 SCFH. The circuit schematic for the temperature monitors and liquid level alarm is shown in Figure 3.5. The liquid level alarm was to insure that the pump did not go dry and overheat.

3.5a Description of Experimental Runs for Phase Two

Three types of packing material were investigated in this study. In Runs One through Three, 7580 3/16-inch polyehtylene spheres purchased from U.S. Plastics were used as a packing material which gave a surface area for bacterial attachment of 5.81 ft^2. The packing was initially seeded by circulating a bacterial suspension through the reactor column for three to four hours a day for several days. When the suspension was not being circulated, the reactor was filled with phenol feed solution to encourage the growth of any attached bacteria. The reactor was continually aerated throughout the total seeding process. The runs were started after two weeks of daily filling the reactor with fresh feed solution and bacterial suspension.

Run Four was to examine the effect of surface area on phenol degradation. More polyethylene spheres were placed into the reactor increasing the surface area for bacterial attachment to 9.20 ft^2. The bed was again seeded using the method described previously.

Very little bacterial slime was evident in the reactor with the polyethylene packing, therefore part of the polyethylene packing was removed

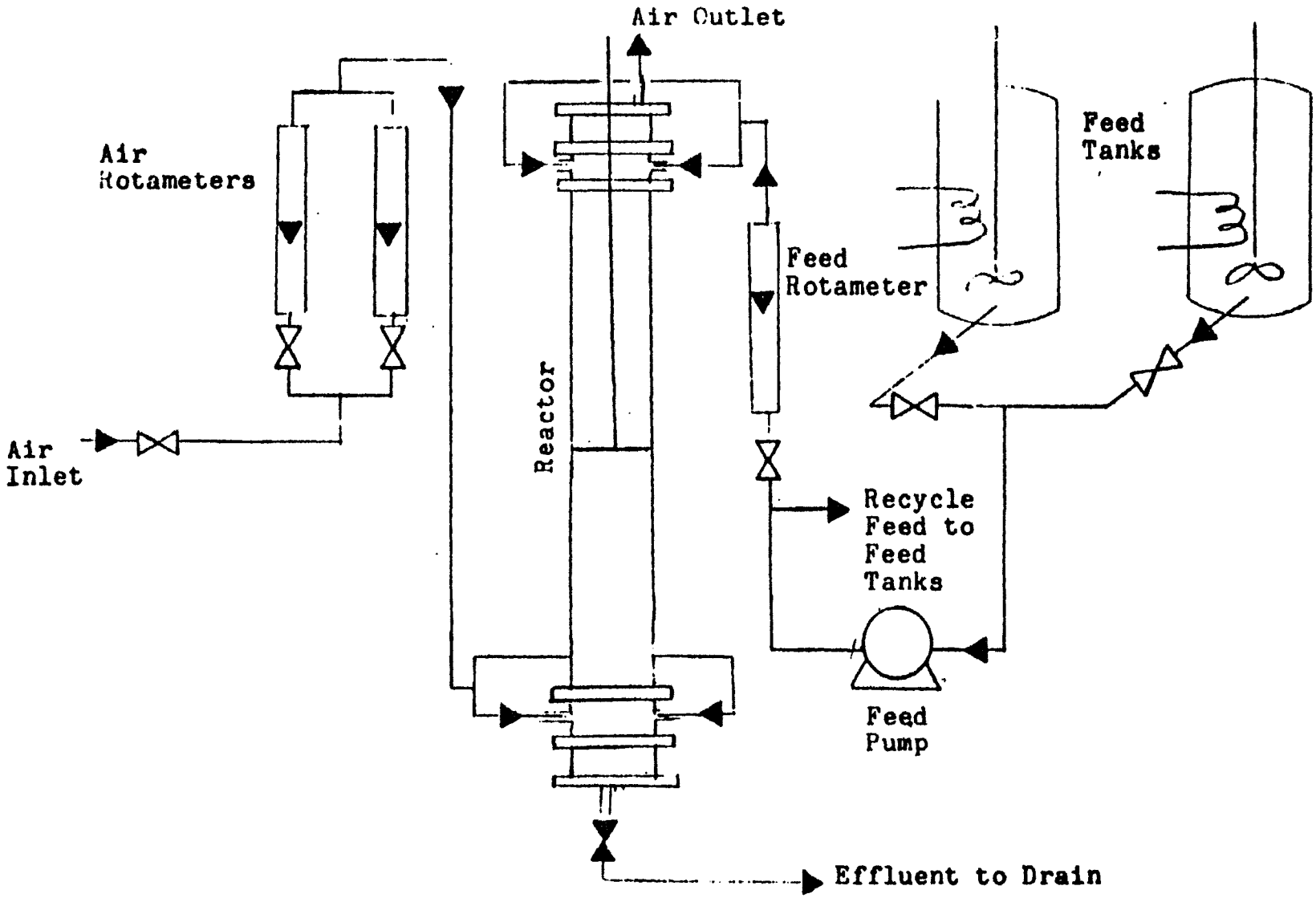

Figure 3.4 Flowsheet for the total reactor system

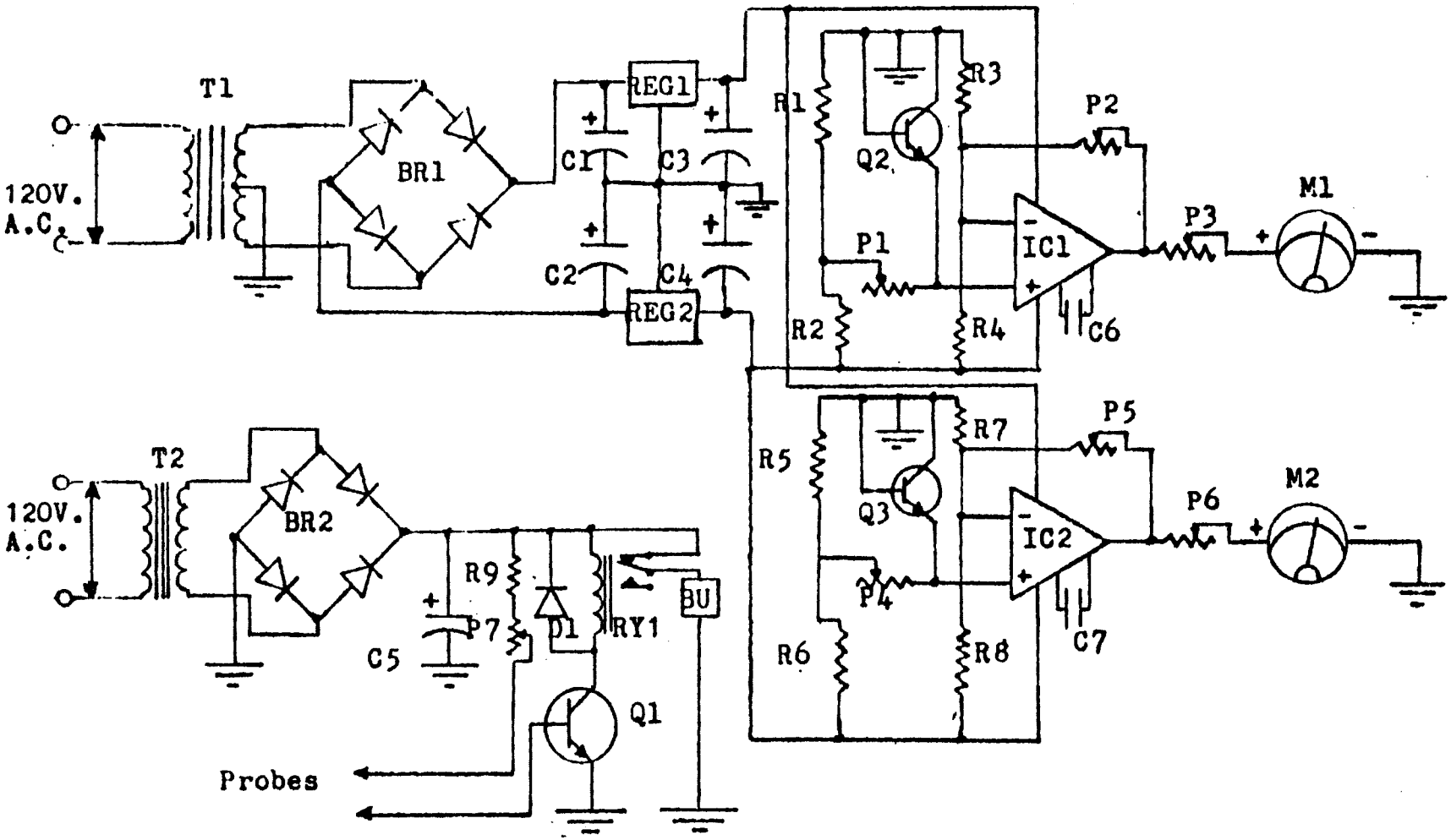

Figure 3.5 Circuit schematic for temperature monitors and liquid level alarm

and 138 g of charcoal (3/8-inch to 1/8-inch size range) was placed into the reactor. Again, the bed was seeded in the method described previously. After several runs, activated sludge (from Columbus Southerly Wastewater Treatment Plant) was added to the reactor. This was done in hope of adding an initial slime coating to the packing and thus promote future bacterial attachment. After 48 hours, the bed was drained and fresh phenol feed and bacterial suspension was added to the bed. After several days of draining and filling the reactor with fresh feed and bacterial solution Run Six was conducted. A heating coil was placed around the reactor at this time also to aid in keeping the reactor at 35°C.

Throughout Runs One through Six the reactor was run in a semifluidized mode, i.e., part of the packing was fluidized and part was packed against either the top retaining grid (Runs Two through Six) or the bottom retaining grid (Run One).

Run Seven was initiated to determine the amount of degradation due to bacterial attachment to the reactor walls and internals. To insure bacterial attachment, the reactor was emptied of all packing. The empty reactor was then filled with feed solution and seeded with a bacterial suspension from the shock culture. After one week of draining and filling with the above mentioned solution, brown floc was evident in sections of the reactor. The bed was sufficiently seeded and readied for further runs.

Packed bed runs were then undertaken with a polypropylene packing to determine the performance of the system. The air flowrate was varied to determine the effect of dissolved oxygen concentration and air shear on phenol degradation. The polypropylene packing used was manufactured by Norton, Inc. under the name of Actifil. The inside diameter of the packing

was 3/4 inch. This type of packing is commonly used in trickling filter wastewater treatment. The packing surface area for bacterial attachment was approximately 5.74 ft^2.

The seeding method for the packing involved cutting the packing into five or six pieces and then floating the packing in flasks containing the stock bacterial solution. The flasks were drained to approximately one-third their initial volume and fresh phenol feed added daily to insure good bacterial growth.

In order to determine the effect of residence time on phenol degradation, a fill-and-draw run was performed. The reactor was filled with fresh phenol feed to 1-1/2 inches above the top retaining grid. This feed was then allowed to remain in the reactor for a set time period. After that time period the reactor was drained and the effluent was analyzed for dissolved oxygen and phenol. This process was repeated using increasing time period.

The flow conditions for the semifluidized runs and packed bed runs are summarized in Tables 3.2 and Table 3.3, respectively.

Table 3.2 - Flow Conditions for Polyethylene Packing and Empty Column Runs

Run No.	Packing Type	Liquid Flowrate (ml/min)	Air Flowrate (SCFH)	Retention Time (min)
1	Polyethylene balls	1514	10	0.94
2	Polyethylene balls	240	10	5.9
3	Polyethylene balls	100	10	14.0
4	Polyethylene balls (amount increased by 37%)	90	10	14.0
5	Polyethylene balls and charcoal	100	5	13.6
6	Polyethylene balls and charcoal (activated sludge added earlier)	100	2	13.6
7	Empty seeded column	100	2	20.2

Table 3.3 - Flow Conditions for Packed Bed Runs*

Run No.	Liquid Flowrate (ml/min)	Air Flowrate (SCFH)	Retention Time (min)
1	100	0	10.2
2	100	2	10.2
3	100	7	10.2
4	100	2	10.2
5	100	2	10.2
6		2	

*Polypropylene packing used for all packed bed runs.

B. Hydrodynamics Study

The schematic diagram of the experimental apparatus for hydrodynamics study is shown in Fig. 3.6. The vertical Plexiglas column in the figure has the dimension of 76.2 mm ID with a maximum height of 2.730 m. The column consists of five sections, namely, the liquid disengagement section, liquid distributor section, test section, gas distributor section and liquid collector section. The liquid and gas distributors which are located at the top and the bottom of the test section, respectively, are designed in such a manner that uniform distributions of liquid and gas can be maintained in the column.

Water and air were used as the liquid and gas in the experiment. Calibrated rotameters were used for the measurements of the gas and liquid flow rates. Pressure taps are evenly spaced at 51 mm intervals on the wall of the test section. The pressure taps were connected to water manometers for the measurement of the static pressure gradient along the column.

In this work, a separate experiment was performed to study the hydrodynamic behavior of the packed bed with countercurrent flow of gas and liquid with the liquid as the continuous phase. This experiment was designed to simulate the hydrodynamic behavior of the packed section in the constrained semifluidized bed. Four different particles, referred to as Particles I - IV, were used in the packed bed experiments, while three different particles, referred to as Particles I - III were used in the constrained fluidized bed experiments and two different particles, referred to as Particles II and III were used in the semifluidized bed experiments. The physical properties of these particles are summarized in Table 3.4. Note that the wall effects may exist in the present system using Particle I in fluidization or semifluidization experiments.

Table 3.4. Summary of physical properties of particles

Particle	Material	d_p (mm)	ρ_s (kg/m^3)
I	polypropylene	9.53	822
II	polyethylene	6.35	930
III	polyethylene	4.76	896
IV	polyethylene	19.05	882

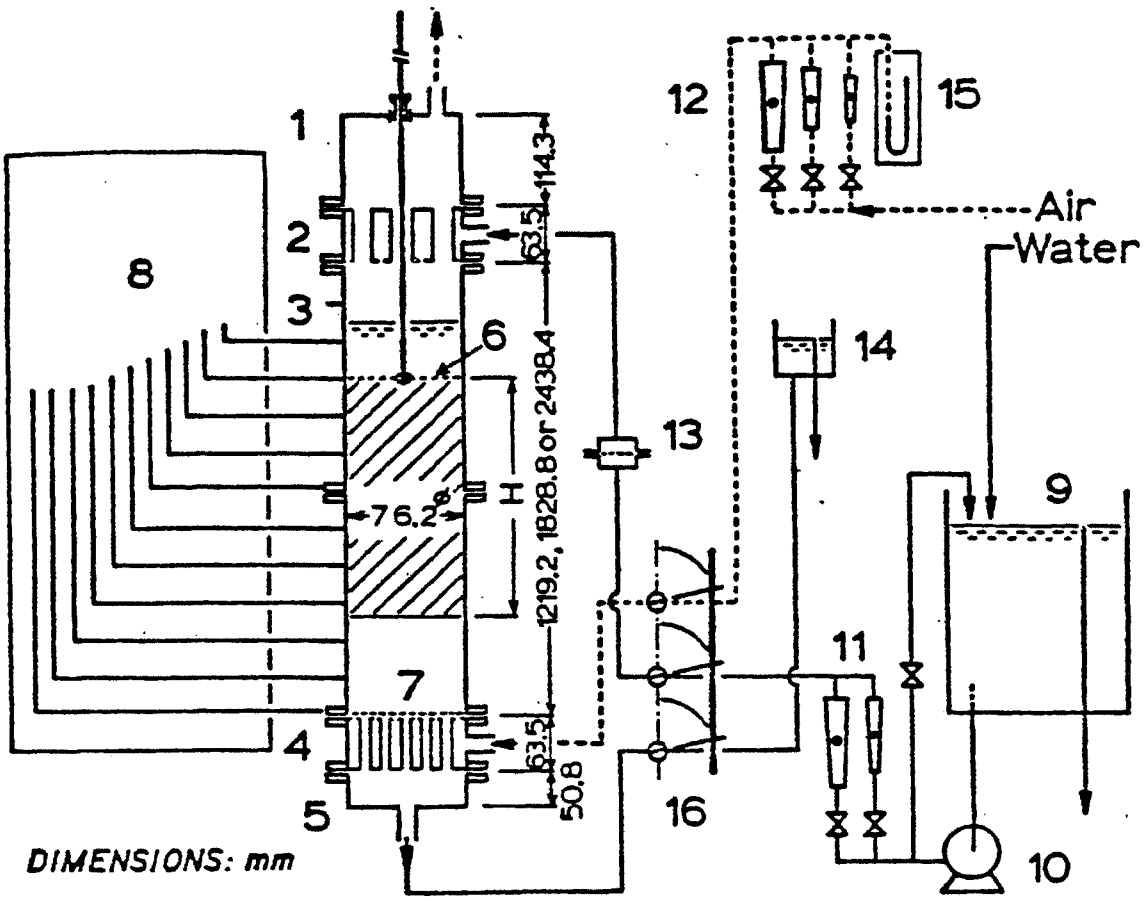

1. Liquid disengagement section
2. Liquid distributor
3. Test section
4. Gas distributor
5. Liquid collector
6. Bed support
7. Wire mesh
8. Manometers
9. Liquid reservoir
10. Liquid pump
11,12. Rotameters
13. Liquid filter
14. Weir
15. Pressure gauge
16. Linked quick closing valve

Figure 3.6 Schematic Diagram of the Experimental Apparatus for Inverse Fluidization in the Gas-Liquid-Solid System

IV. RESULTS AND DISCUSSION

A. Biological Study

4.1a Acclimation of phenol bacteria

The batch study chemical analysis results are shown in Figure 4.1 through 4.8. Figure 4.1 shows the rate of phenol degradation for the control solutions consisting of 100 ml distilled water to three liters phenol feed. In Figure 4.5 and 45°C control exhibits early contamination while the 24°C and 35°C controls show later contamination. When comparing the controls with the bacteria solution consisting of 100 ml bacterial suspension to three liters phenol feed, it can be seen that the bacterial solutions degraded the phenol much quicker than the control solutions (see Figure 4.2 and Figure 4.5). The controls (except for the 45°C control) exhibit only a slight change in phenol concentration and COD over the time period dur ng which the phenol concentration of the bacterial solution decreased rapidly to 0 mg/L. Figure 4.6 shows that the majority of COD depletion occurred over the same time period as the phenol degradation; therefore, it can be deduced that the majority of the COD is due to the phenol concentration. All of the controls were eventually contaminated due to the resulting splashing from aerating the solutions.

Further runs were conducted to determine the effects of temperature on phenol degradation rates since this was not evident at the lower phenol concentration level. Initial phenol concentrations of approximately 450 mg/L and 650 mg/L were used. The degradation rates of these studies are shown in Figures 4.3, 4.4, 4.7, and 4.8. At the 450 mg/L level, the maximum rate of phenol degradation occurs at 45°C. More decisive results were seen at the 650 mg/L level. At this initial concentration level the effects of concentration as well as temperature can be observed. The bacteria in the 45°C

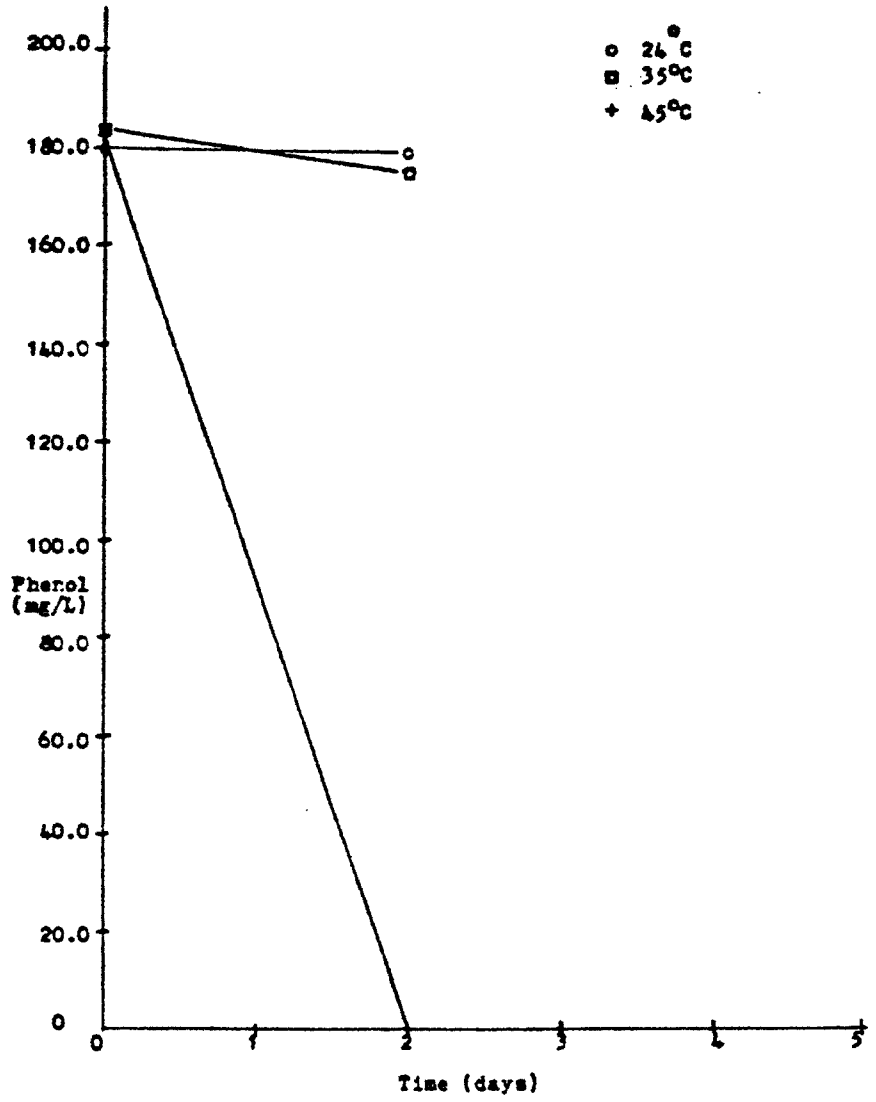

Figure 4.1 Control group phenol degradation curve for initial phenol concentration of approximately 200 mg/L

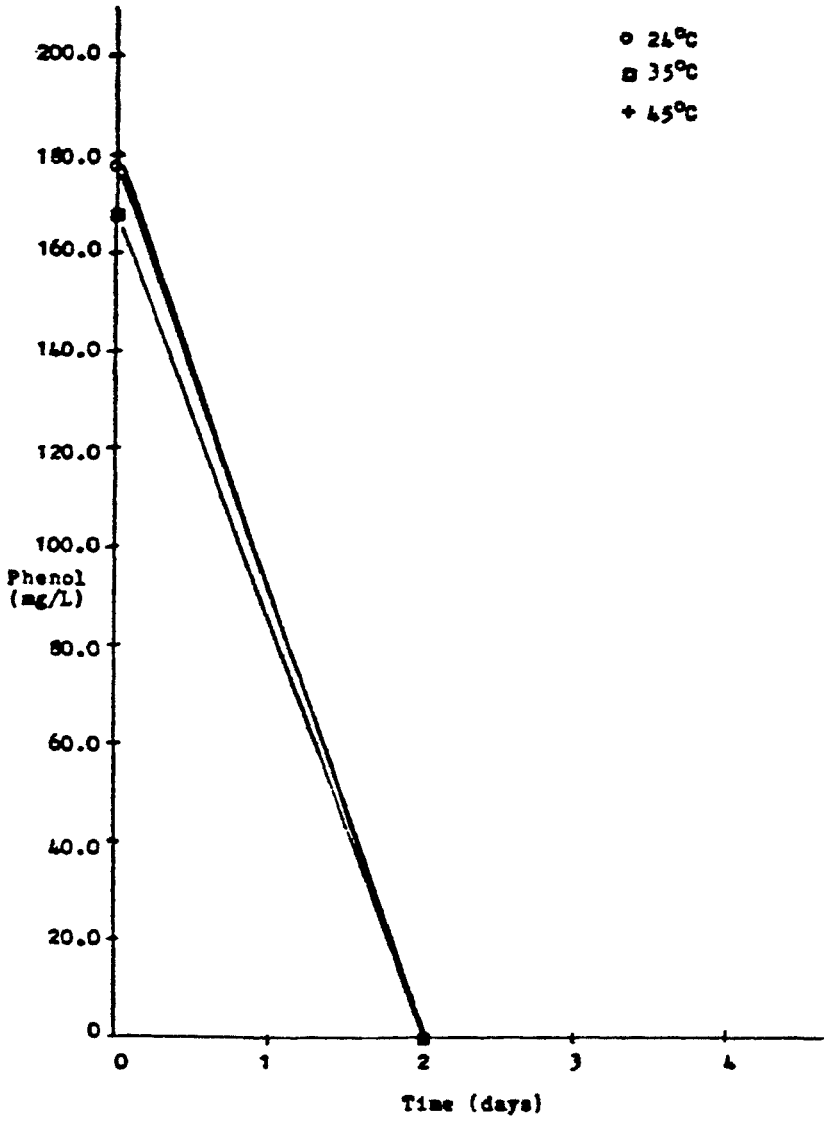

Figure 4.2 Sample group phenol degradation curve for initial phenol concentration of approximately 200 mg/L

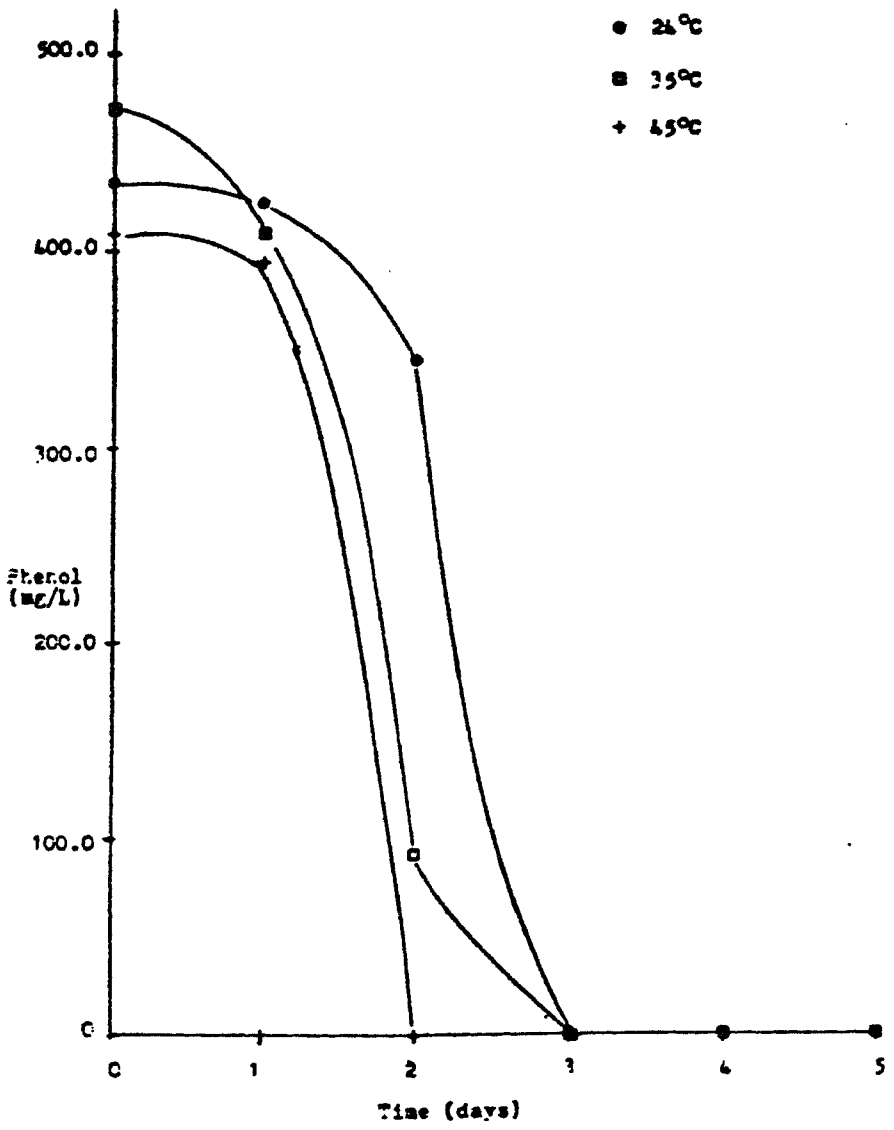

Figure 4.3 Sample group phenol degradation curve for initial phenol concentration of approximately 450 mg/L

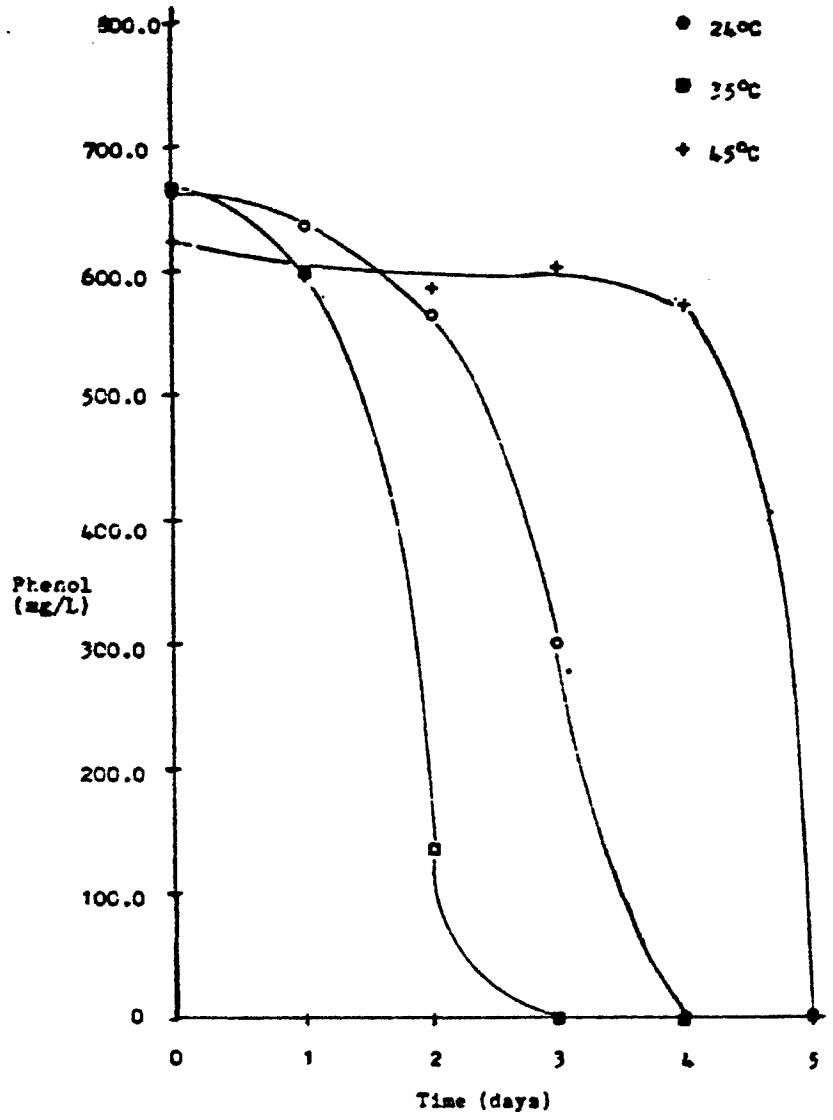

Figure 4.4 Sample group phenol degradation curve for initial phenol concentration of approximately 650 mg/L

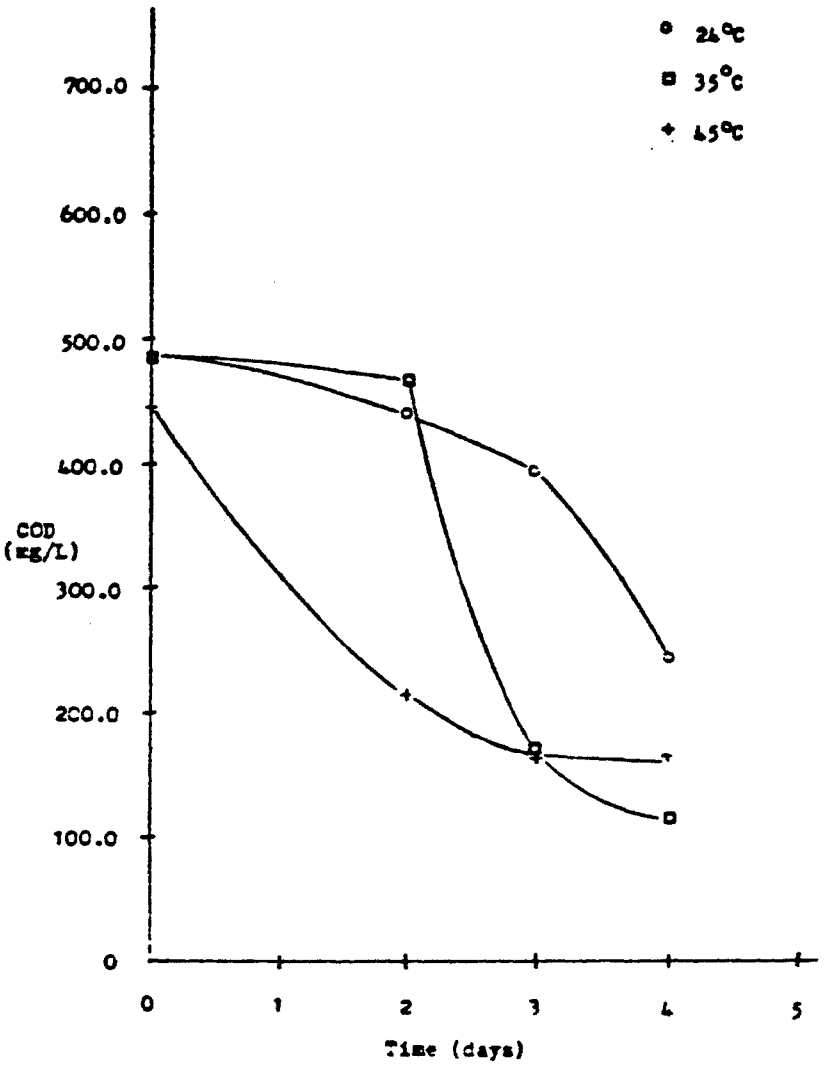

Figure 4.5 Control group COD (Chemical Oxygen Demand) depletion curve for initial phenol concentration of approximately 200 mg/L

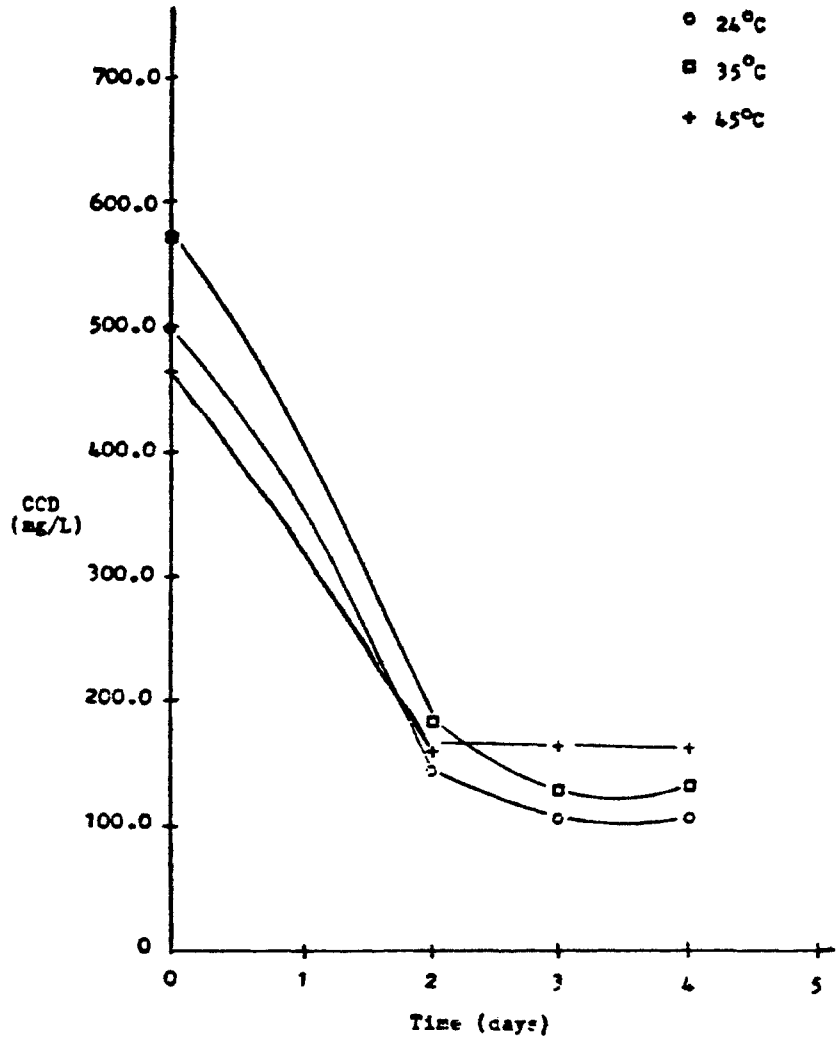

Figure 4.6 Sample group COD depletion curve for initial phenol concentration of approximately 200 mg/L

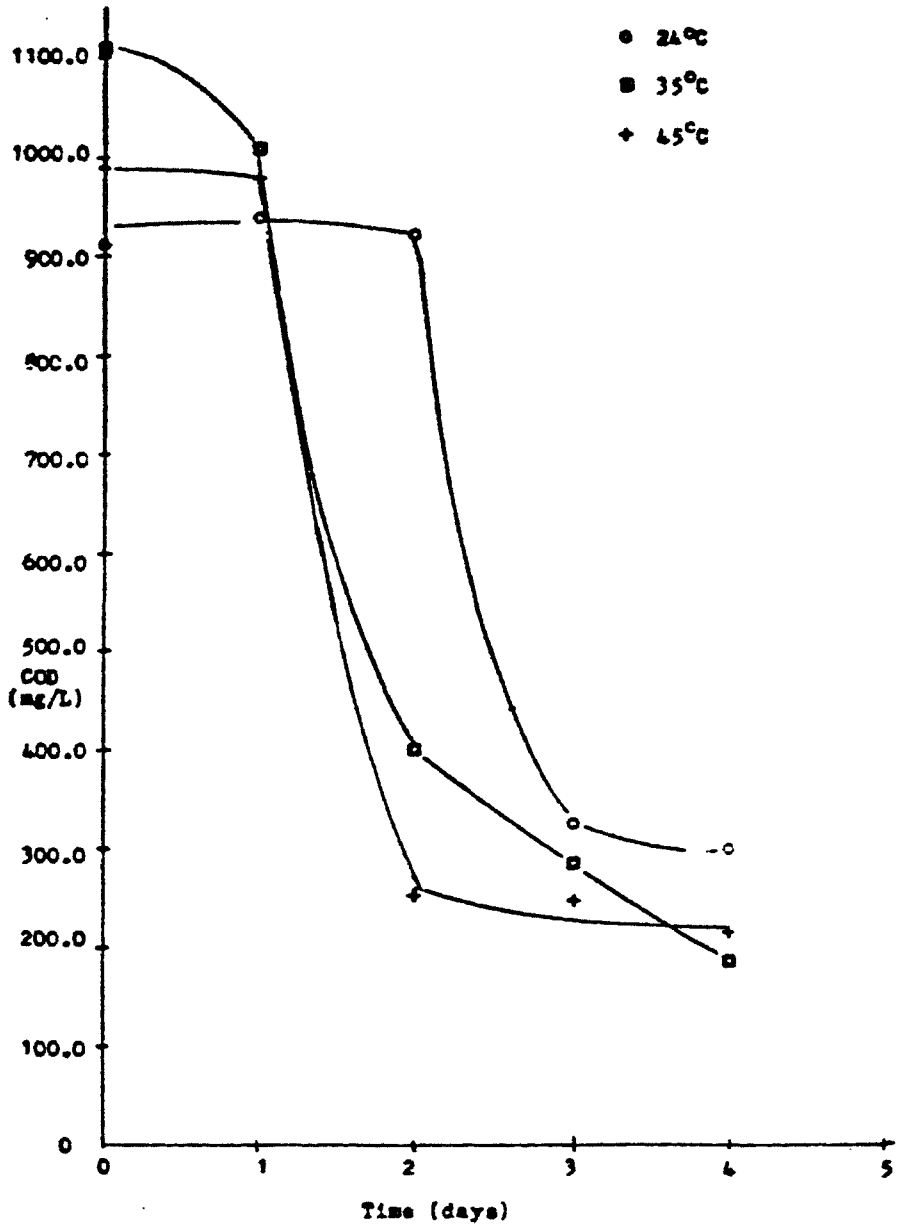

Figure 4.7 Sample group COD depletion curve for initial phenol concentration of approximately 450 mg/L

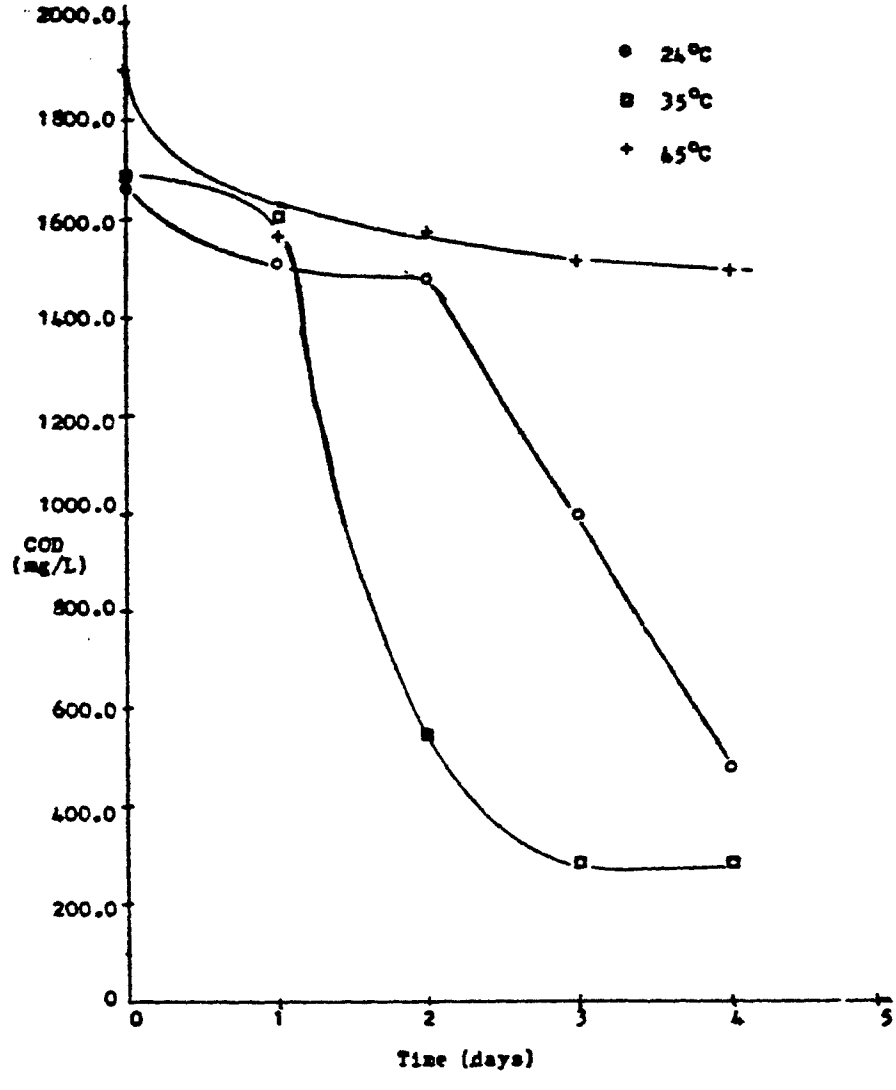

Figure 4.8 Sample group COD depletion curve for initial phenol concentration of approximately 650 mg/L

culture appear to be inhibited by the higher phenol concentration while the bacteria at 24°C and 35°C do not appear to be as radically affected by the higher phenol concentration. Higher phenol concentrations were not attempted due to the difficulty in dissolving the solid phenol in the feed solution. Controls were not run at the higher phenol concentration levels since the controls at the 200 mg/L level showed adequately that the degradation was due to bacterial action and not to other parameters.

All the figures show a close correlation in decreasing trends between phenol concentrations and COD. The COD should not reduce to zero since the bacterial biomass contributes to the COD. However, the decreasing COD shows loss of carbon due to bacterial respiration of carbon dioxide.

It is interesting to note the physical differences in the three mixed bacterial cultures. The culture at 45°C did not form a floc but stayed in a milky colored colloidal suspension. The cultures at 24°C and 35°C formed a heavy floc which quickly settled and the solutions turned to a golden yellow color after several days.

4.2a Semifluidized Bed and Packed Bed Run

Semifluidized Bed Runs

The influent and effluent concentrations for the semifluidized bed runs are summarized in Table 4.1. Throughout Runs One through Six, very little bacterial growth was visually evident in the reactor.

The results from Runs One through Three are shown graphically in Figure 4.9. As expected, decreased liquid flowrate and, as a result, increased retention time increased the amount of phenol degradation.

In an attempt to further increase the amount of phenol degradation, the

Table 4.1 - Phenol Degradation Using Polyethylene Packing

Run	Packing Type	Phenol Concentration Influent (mg/L)	Effluent (mg/L)	$C_{in} - C_{eff}$ (mg/L)	Degradation Rate* (g/L-day)
1	Polyethylene balls	46.2	44.5	1.7	2.28
2	Polyethylene balls	50.4	47.0	3.4	0.83
3	Polyethylene balls	47.3	40.8	6.4	0.65
4	Polyethylene balls	47.0	41.8	5.2	0.59
5	Polyethylene balls and charcoal	68.0	60.3	7.7	0.82
6	Polyethylene balls and charcoal (activated sludge added)	48.2	42.9	5.3	0.56
7	Empty seeded column	52.2	50.2	2.0	0.14

*Based on filled reactor volume.

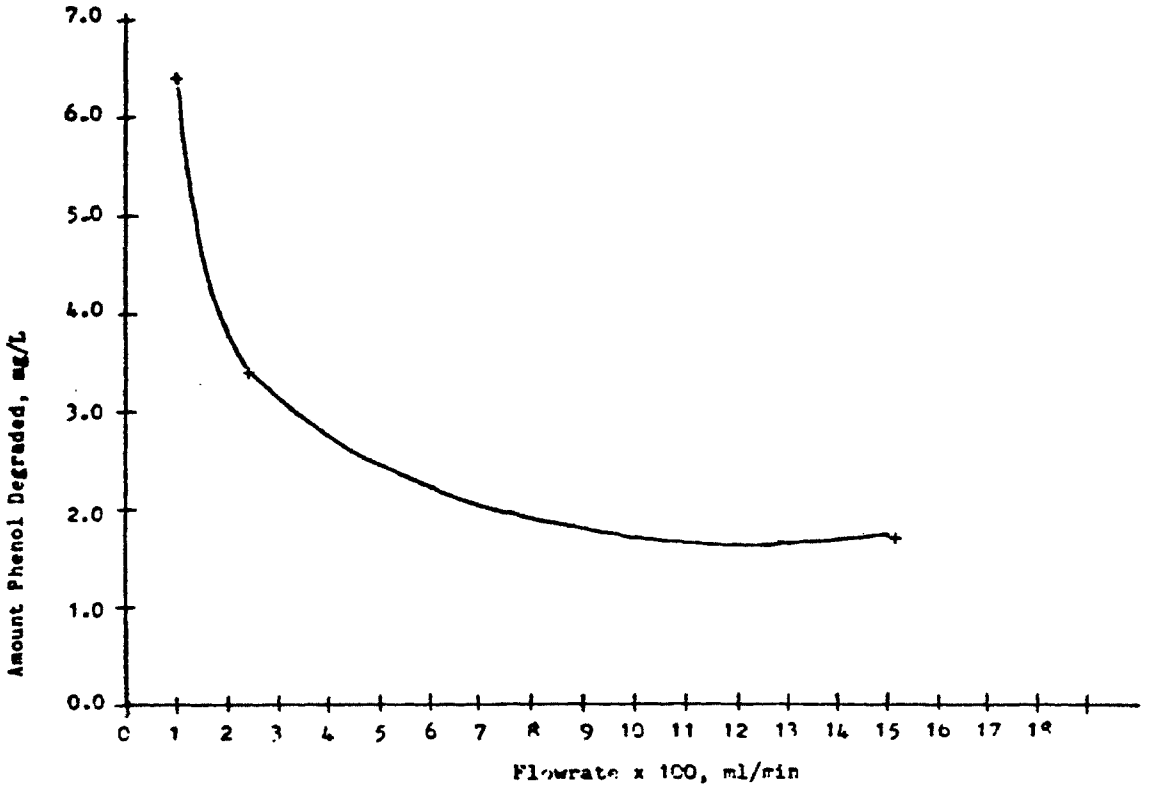

Figure 4.9 The effect of increased liquid flowrate on the amount of phenol degraded using polyethylene ball packing

available surface area for bacterial attachment was increased in Run Four by increasing the amount of polyethylene packing used in the reactor. The increase in surface area, however, did not increase the phenol degradation. This was probably due to poor bacterial attachment to the polyethylene balls. Extending the period of time used for seeding and establishing the bacterial slime on the packing may possibly yield higher degradation rates. However, this was not pursued any further.

In Runs Five and Six, charcoal was used as a packing material. The polyethylene spheres were used as an aid in fluidizing the charcoal. The spheres did not work as well as anticipated since the majority of the charcoal eventually gained weight and packed against the bottom retaining grid. The charcoal therefore was discarded because of its inability to fluidize. No brown bacterial growth was evident on the charcoal particles even though the amount of phenol degraded increased slightly as can be seen in Table 4.1.

An initial coating of bacteria onto a surface is necessary before heavy slime formation will take place. Due to the small amount of phenol degradation, it was proposed that this initial formation may have not taken place throughout the bed. In order to greatly increase the amount of bacteria in the bed and thus promote attachment, activated sludge was added to the bed. As can be seen by the results of Run Six, either the attachment did not increase or the bacterial attachment was not the reason for low phenol degradation rates.

As seen from the raw data in Appendix C, Run Four took the longest time to reach steady state. The transient phenol concentrations for Run Four can be seen in Figure 4.10. In Run Four the reactor reached steady state after about one hour whereas in the other runs the reactor reached steady state after 45 minutes.

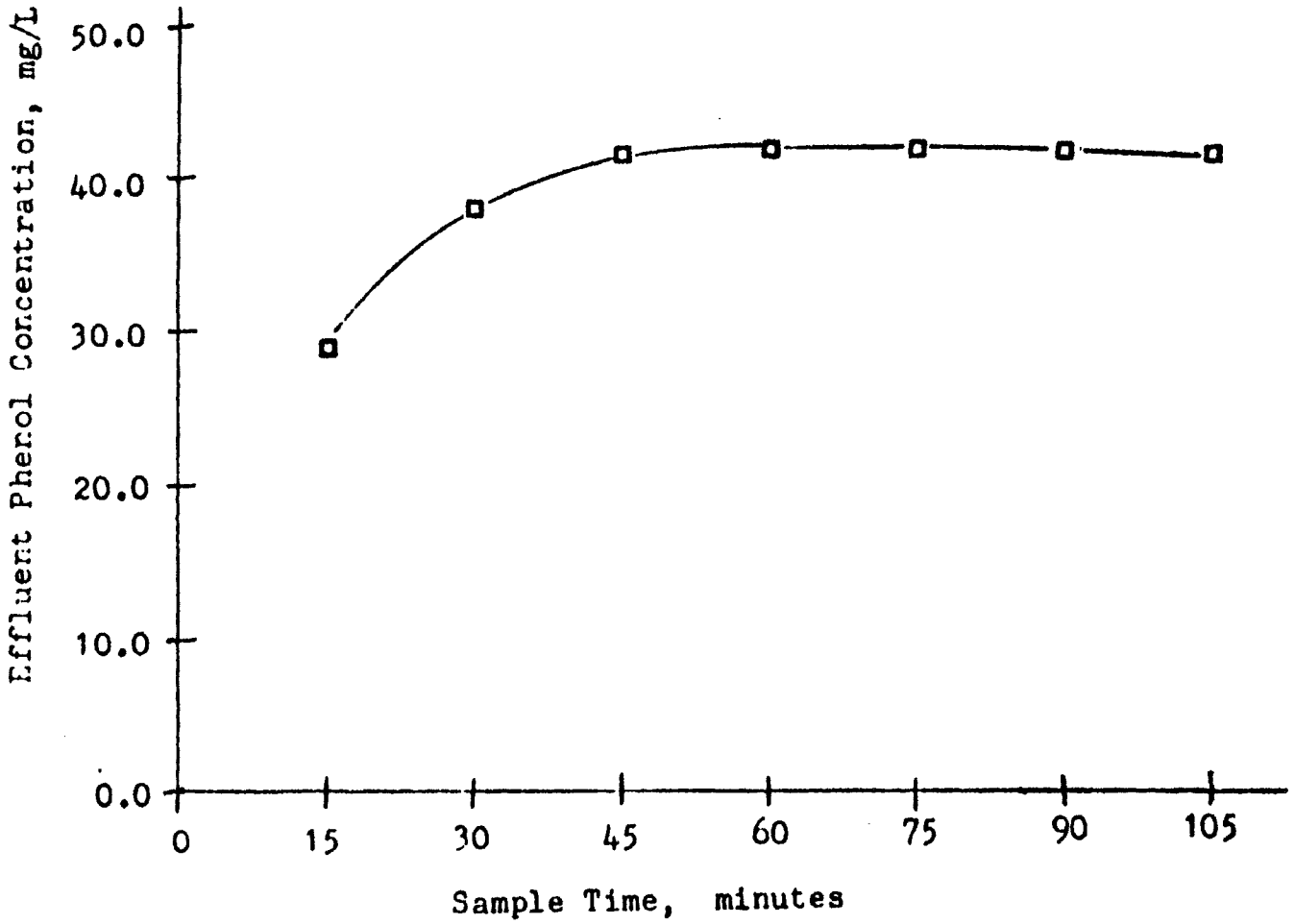

Figure 4.10 Transient data for Run Four

No effluent samples were taken from the reactor prior to startup. The initial effluent concentration can be assume to be very close to 0 mg/L. This will be explained in greater detail in the next section.

An empty column run was initiated in order to determine the approximate amount of phenol degradation due solely to the bacteria attached to the reactor walls and internals. Brown floc was observed clinging to the inside surfaces of the reactor. The resulting phenol degradation of 2.0 mg/L (see Table 4.1) should be considered the peak phenol degradation solely due to wall attachment since the extent of bacteria growth was not as evident during any of the previous runs. The retention time for the empty column run was also much higher than the previous runs (see Table 3.2). The higher retention time increased the amount of phenol degradation. From the result of Run Seven, it can be seen that most of the phenol degradation was due to either bacterial attachment or entrapment in the packing.

Packed Bed Runs

The packed bed runs were conducted to better understand the bacterial system used in the study. Bacterial growth was evident on the polypropylene packing. The bacterial slime growth appeared to be heaviest in the middle of the packed section. The section of packing closest to the air distribution plate showed minimal bacterial growth due most likely to air shearing. The effect of air flowrate and dissolved oxygen concentration on the amount of phenol degraded was investigated. Table 4.2 shows the effect for similar influent phenol concentrations of increased flowrate on the amount of phenol degraded. High air flowrates increased the amount of phenol degraded to a slight degree. This data, however, due to the low amount of phenol degraded,

Table 4.2 - Results of Packed Bed Runs*

Run	Phenol Concentration Influent (mg/L)	Effluent (mg/L)	Amt. Phenol Degraded (mg/L)	Degradation Rate (g/L-day)	Air Flowrate SCFH
1	48.6	44.4/	4.2	0.55	0
4	47.8	44.8	3.0	0.39	2
3	47.35	41.5	5.85	0.76	7

*Polypropylene packing used for all runs.

does not give conclusive evidence on the effect of air flow rates on phenol degradation. Transient data for Runs One, Three, and Four is shown in Figures 4.11, 4.12, and 4.13, respectively. Similar trends can be seen for all three runs. The low effluent concentration during the early sample times was due to the sampling procedure. Instead of the reactor being emptied and filled with fresh feed solution at the onset of the experimental runs, the feed solution that was left overnight in the reactor was run out during the beginning of the run while fresh feed was entering the reactor. Since the feed soltuion left overnight in the reactor had a very low phenol concentration, the mixing of the spent feed solution with the fresh feed resulted in low effluent phenol concentrations. After approximately 90 minutes of operation all of the spent feed solution was flushed from the reactor. As a result, the effluent phenol concentration leveled off.

Experimental runs using a lower influent phenol concentration of approximately 30 mg/L, as opposed to 50 mg/L in the previous runs, were conducted to determine what effect influent phenol concentration would have on the amount of phenol degraded. The results of these runs can be seen in Figure 4.14 and Figure 4.15. Poor mixing in the feed tanks would explain the decreasing influent phenol concentrations evident in these figures. When the liquid level in the feed tank became low, the mixers could not adequately keep a uniform solution. These runs do show that at lower influent phenol concentrations more phenol is degraded. This could be due to an inhibition of the phenol degrading ability of the bacteria at high phenol concentrations.

The effect of retention time on phenol degradation was investigated by

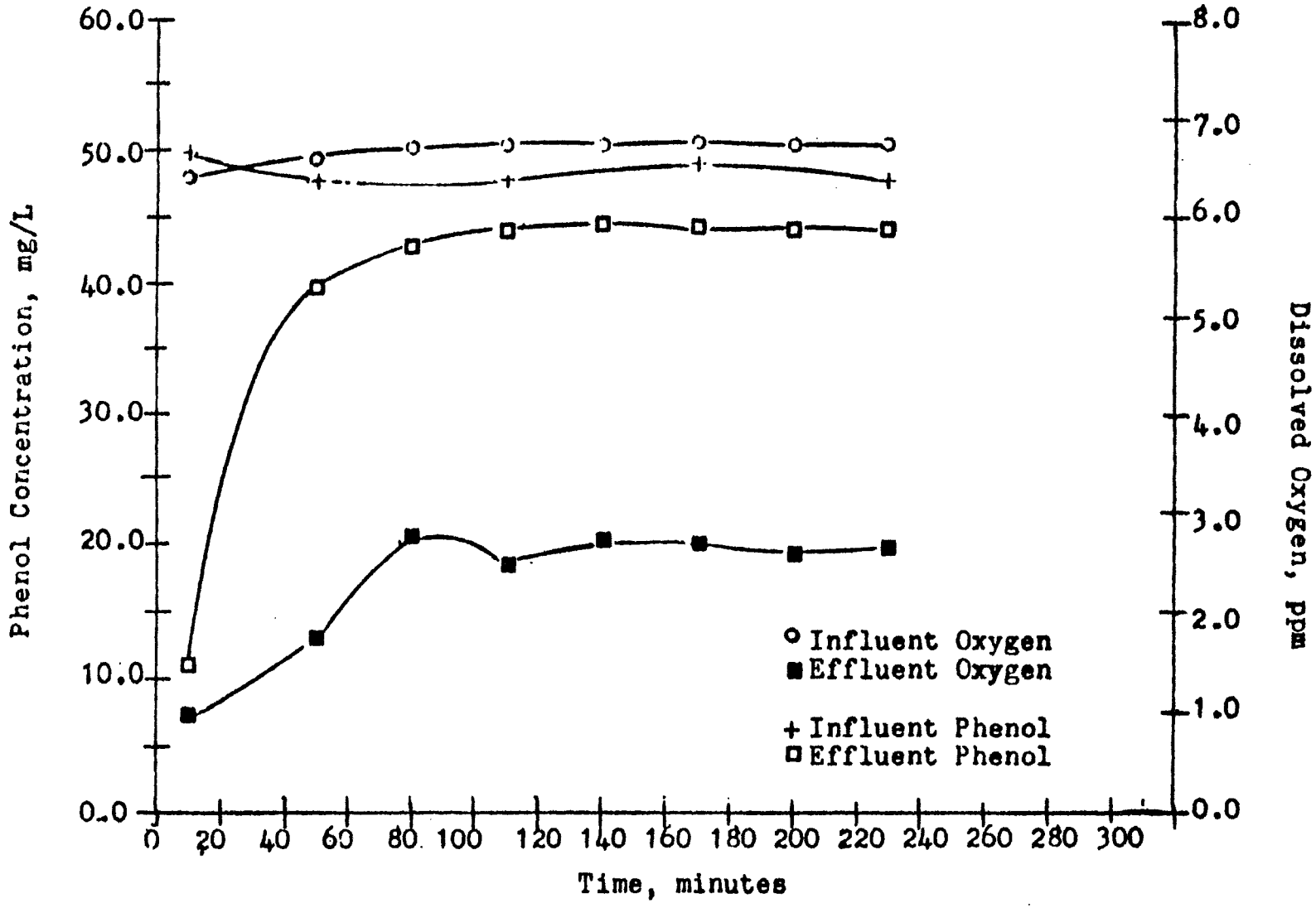

Figure 4.11 Transient data for packed bed Run One (airflow 0 SCFH)

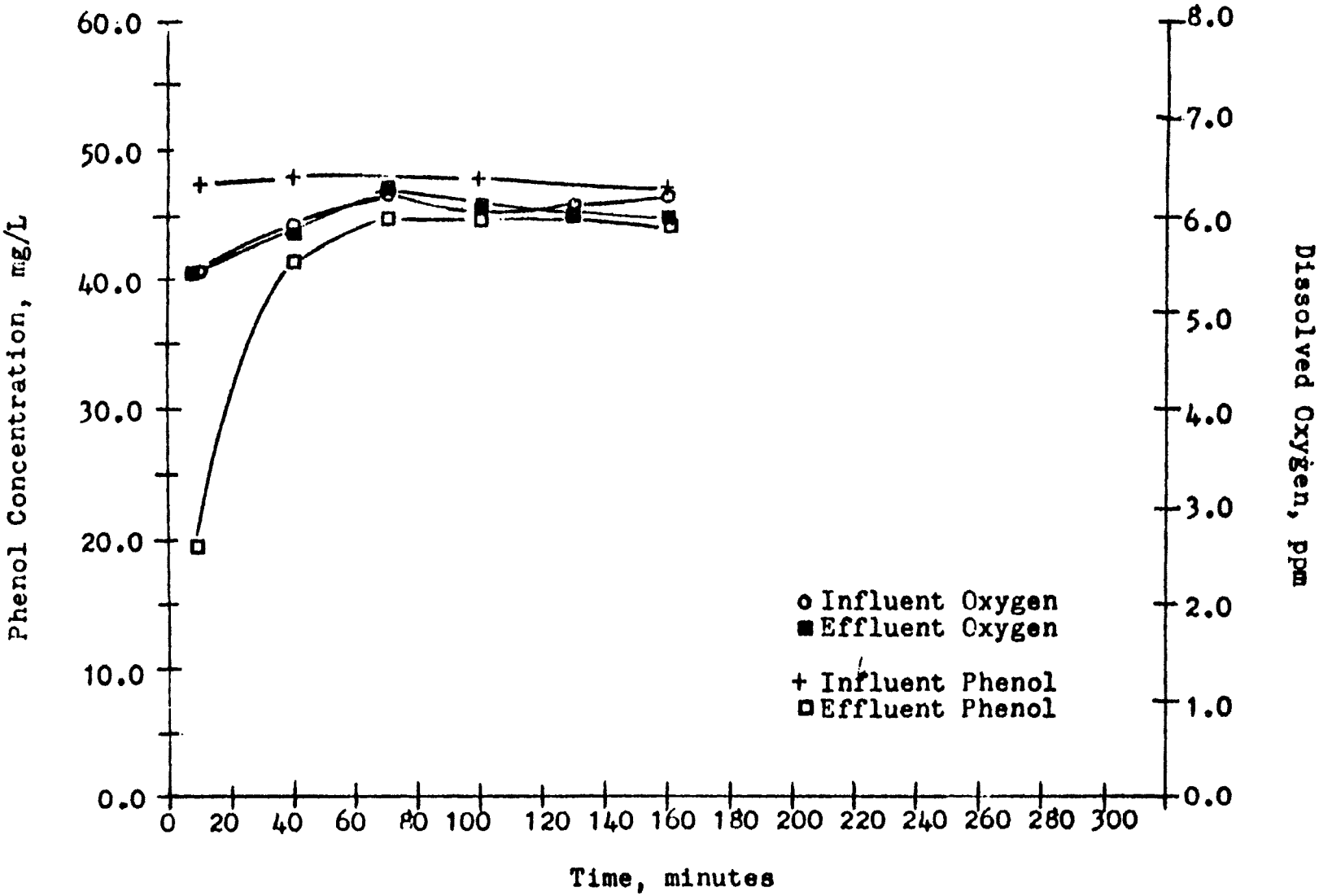

Figure 4.12 Transient data for packed bed Run Four (airflow 2 SCFH)

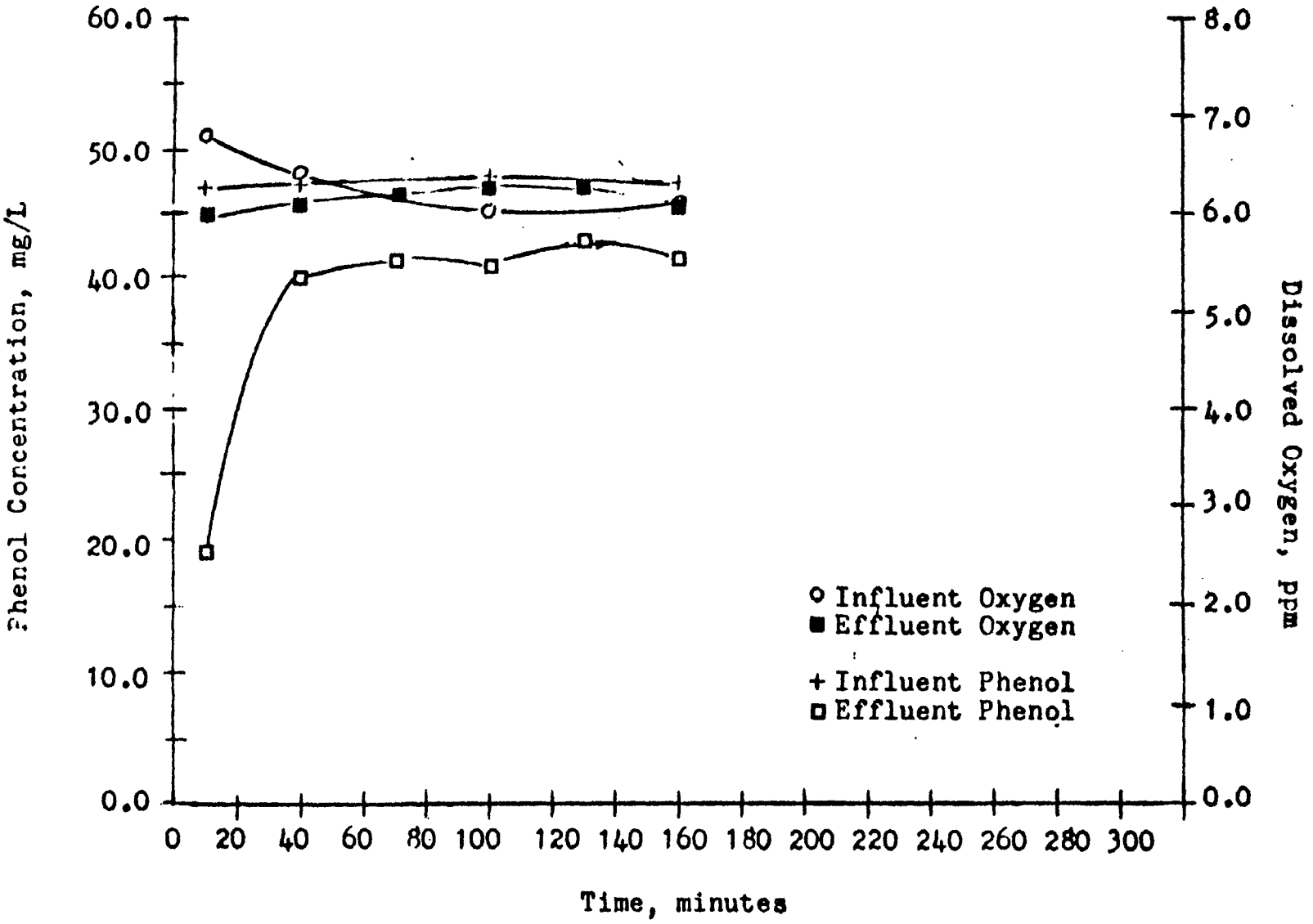

Figure 4.13 Transient response of packed bed Run Three (airflow 7 SCFH)

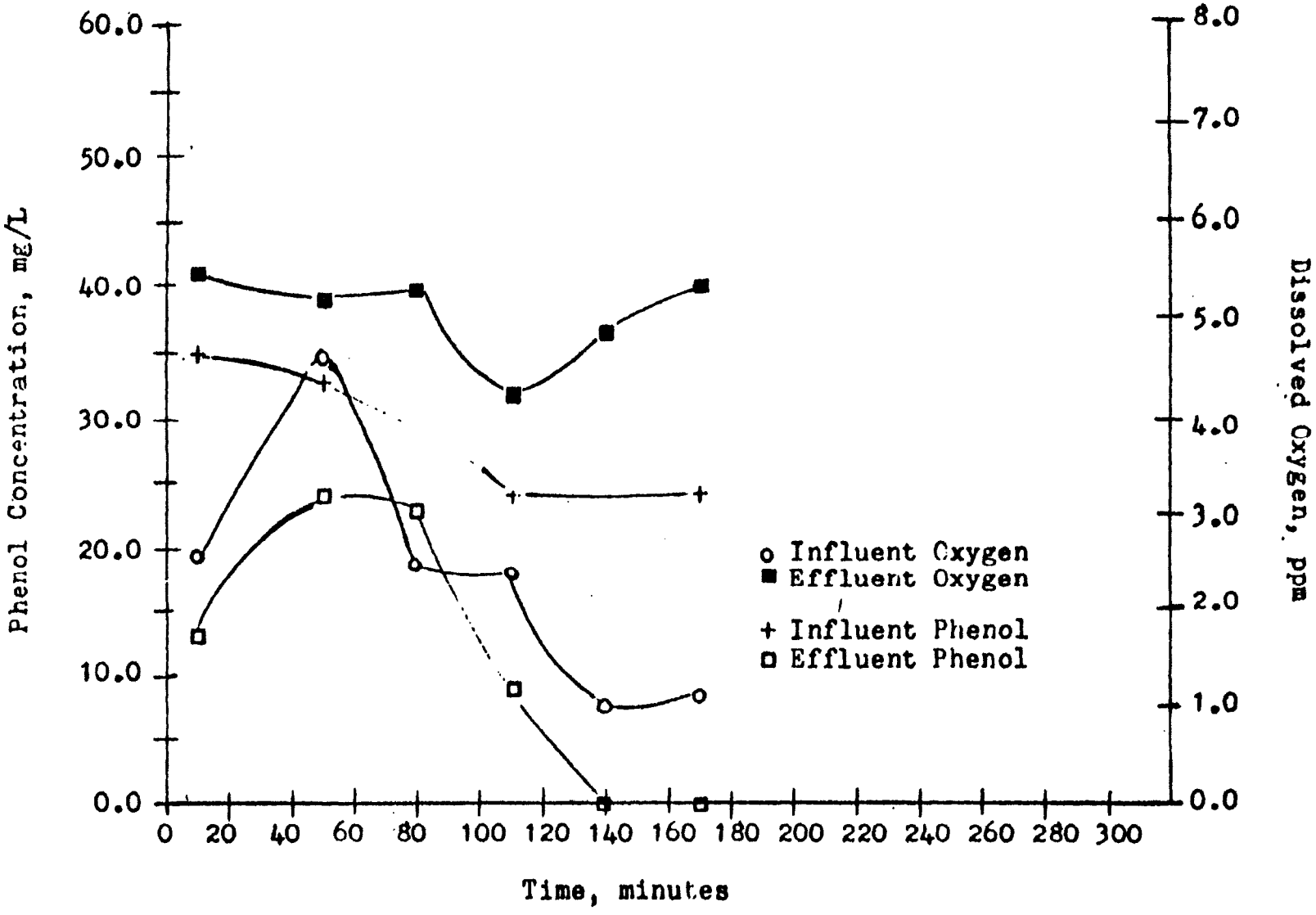

Figure 4.14 Transient response of packed bed Run Two (airflow 2 SCFH)

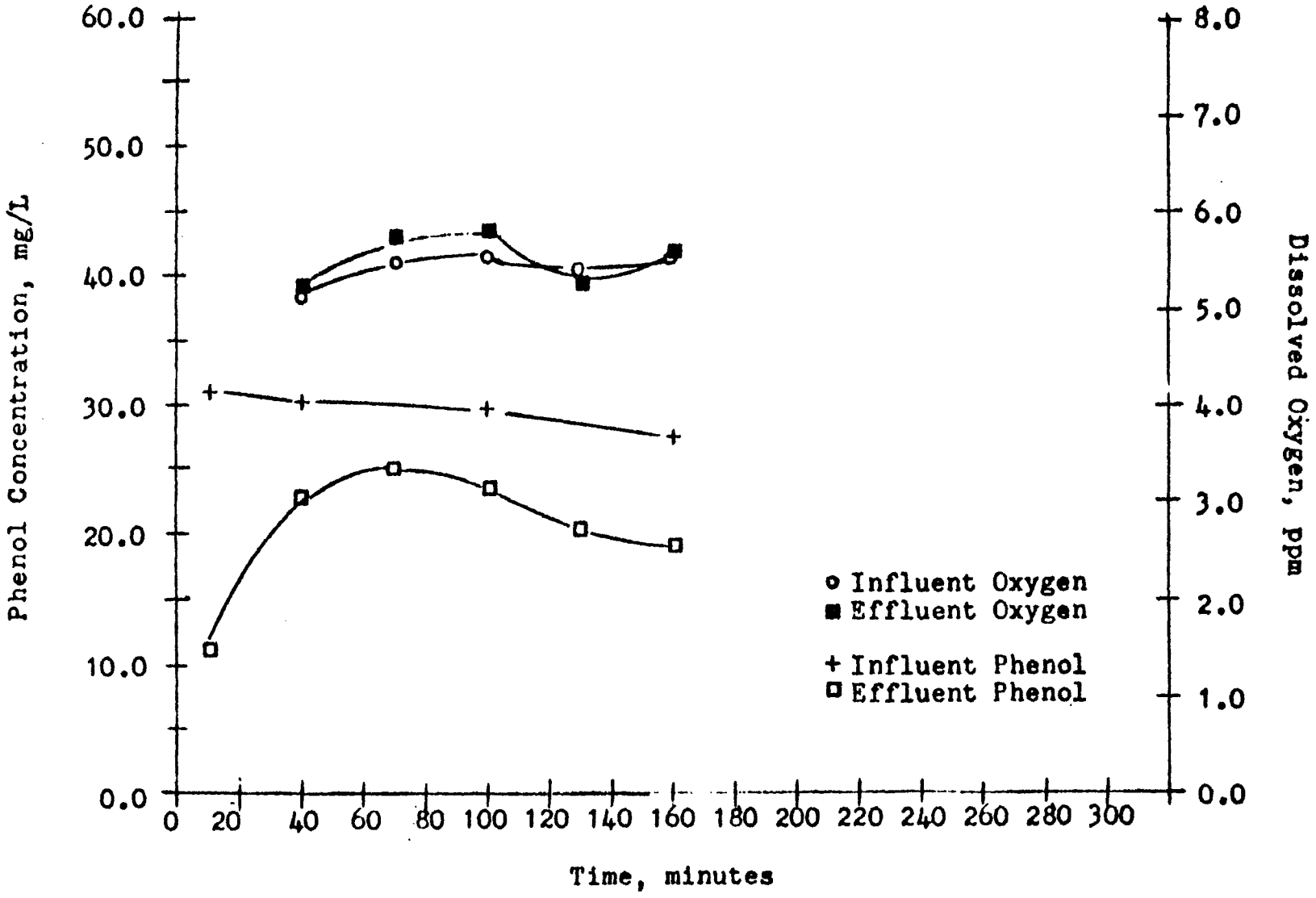

Figure 4.15 Transient response of packed bed Run Five (airflow 2 SCFH)

using a fill and draw system of sampling. The results from this run can be seen in Figure 4.16. By filling the reactor with fresh feed solution, letting the solution remain in the reactor for a predetermined time period, and then sampling after this time period was over, a continuous flow system (assuming a very low liquid flowrate) could be approximated. The effect of influent phenol concentratin on degradation rate can be explained from Figure 4.16 using the effluent concentration curve. A retention time of approximately 20 minutes is required to decrease the effluent phenol concentration from 45 mg/L to 40 mg/L. However, to decrease the phenol concentration from 25 mg/L to 20 mg/L at retention time of only 3 minutes is needed.

The increased phenol degradation at lower phenol concentrations could be due to one or both of the following factors.

1. High phenol concentrations could inhibit the degrading ability of the bacteria. As the phenol concentration decreases, the inhibition decreases and thus more phenol is degraded in a shorter time period.

2. Time is required for the bacteria to produce the enzymes needed to degrade the phenol. At long retention times, the time to produce the enzymes is adequate where at short retetnion times, there is little time to produce the necessary enzymes. It is interesting to note that at a retention time of 30 minutes, 15 mg/L phenol is degraded while at a retention time of 45 minutes 27.6 mg/L phenol is degraded

The inhibiting phenol concentration has not been well established at this time. Yang and Humphrey (61) using Pseudomonas putida and Trichosporon cutaneum (a yeast) observed phenol inhibition at phenol concentrations above 100 mg/L. Lee et al. (40) observed that the phenol degrading bacteria could tolerate phenol levels in excess of 1500 mg/L on a temporary basis. However, at levels above 200 mg/L, the degradation rates began to fall, which Lee, et al. concluded was due to substrate inhibition. Holladay, et al. (32) used a phenol concentration of 2200 mg/L for several fluidized

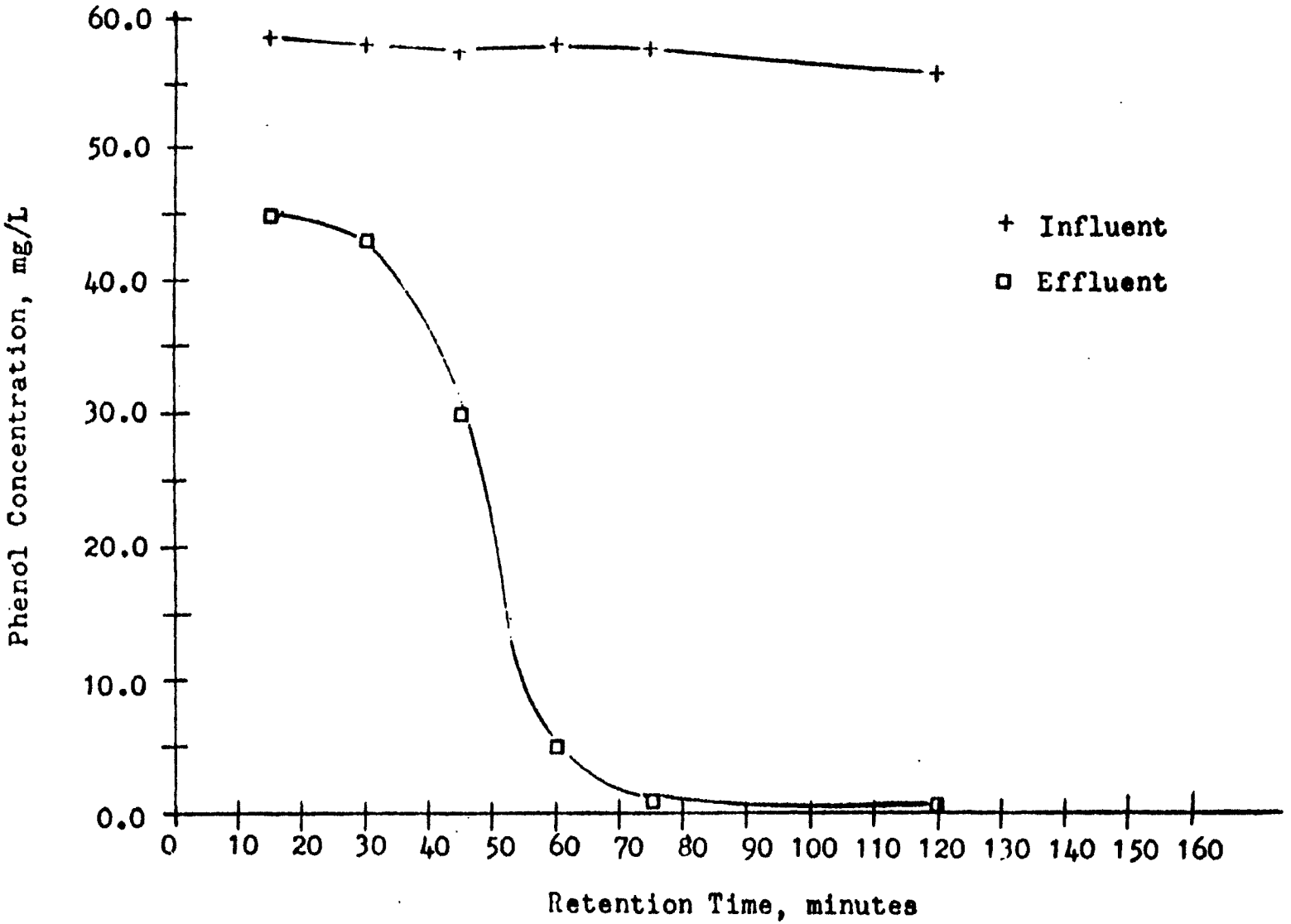

Figure 4.16 Effect of retention time on phenol degradation (fill and draw samples)

bed runs; however, this feed concentration resulted in decimation of the microorganism population after only a few days. Holladay et al. suggested a reasonable influent phenol operating range to be from 100 mg/L to 700 mg/L.

The batch studies from Phase One can be compared and contrasted with the results from the fill and draw sample run. Much more bacterial growth was present in the packed bed than in the batch system; thus, phenol can be degraded quicker in a packed bed system. The amount of time needed to degrade 450 mg/L phenol in the batch system does give a high estimation of the retention time needed to degrade 450 mg/L in the packed bed system.

B. Hydrodynamics Study

4.1b Packed Bed Behavior

The first and last pressure taps used for the pressure measurement were located 5.1 cm from the bottom and the top of the packed bed, respectively, in order to avoid end effects. The pressure drops in the packed bed were calculated from manometer readings.

The mathematical model accounting for the pressure drop in the packed bed considers that the gas and liquid flows are one-dimensional and the solid particles can be completely wetted by the liquid and, thus, there is no direct contact between the gas and solid at any instant of fluidization. Under such a condition, the system is viewed to be represented by three distinct phases, i.e., gas, liquid, and solid phases, with the gas phase in the core area, the solid phase in the wall area and the liquid phase between the core and wall areas. The schematic representation of the model is given in Fig. 4.17. The boundary between the liquid and gas phase is defined in the model by an equivalent radius R_2, while that between the liquid and solid

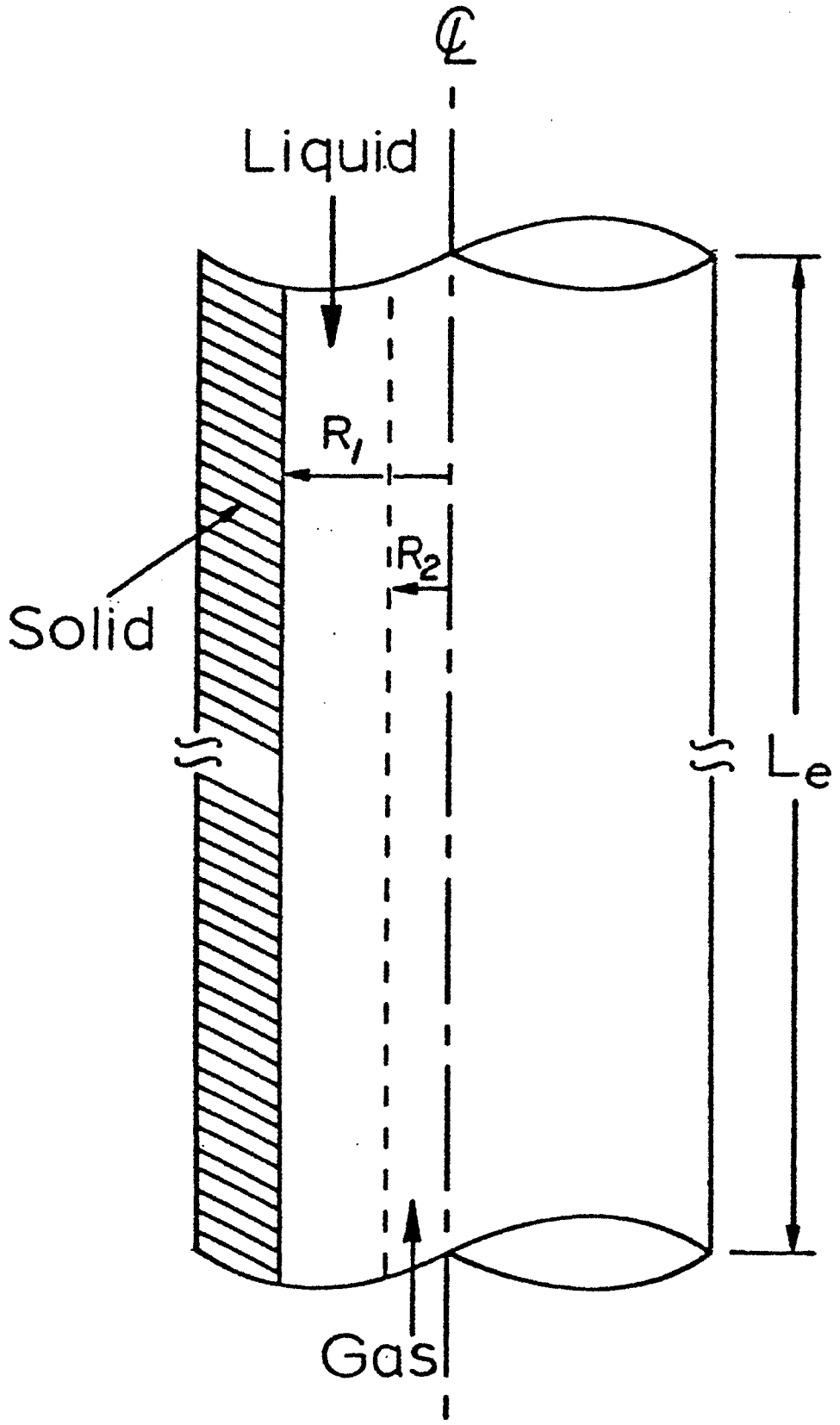

Fig. 4.17. Schematic Representation of the Model.

phases is defined by an equivalent radius R_1. The values for R_1 and R_2 can be determined in the following manner: The liquid volume in the system can be expressed by

$$(\frac{\pi}{4} D^2)\ (H_{pa})\ (\varepsilon_\ell{}^p) = \pi(R_1{}^2 - R_2{}^2)\ (L_e) \tag{1}$$

The gas volume in the system can be expressed by

$$(\frac{\pi}{4} D^2)\ (H_{pa})\ (\varepsilon_g{}^p) = (\pi R_2{}^2)\ (L_e) \tag{2}$$

From Eqns. (1) and (2), we have

$$\frac{\varepsilon_\ell{}^p}{\varepsilon_g{}^p} = \frac{R_1{}^2 - R_2{}^2}{R_2{}^2} \tag{3}$$

or

$$\frac{R_1}{R_2} = \sqrt{1 + \frac{\varepsilon_\ell{}^p}{\varepsilon_g{}^p}} \tag{4}$$

The liquid-solid interfacial area can be given by

$$(2\pi R_1)(L_e) = (\frac{\pi}{4} D^2)(H_{pa})(\varepsilon_s{}^p)(\frac{6}{d_p}) \tag{5}$$

Thus, we have

$$R_1 L_e = \frac{3}{4} \frac{D^2 H_{pa}\ \varepsilon_s{}^p}{d_p} \tag{6}$$

Combining Eqns. (2), (4), and (6) yields

$$R_2 = \frac{\varepsilon_g{}^p\ d_p}{3\varepsilon_s{}^p} \sqrt{1 + \frac{\varepsilon_\ell{}^p}{\varepsilon_g{}^p}} \tag{7}$$

Equations (4) and (7) yields

$$R_1 = \frac{\varepsilon_g{}^p d_p}{3\varepsilon_s{}^p} \left(1 + \frac{\varepsilon_\ell{}^p}{\varepsilon_g{}^p}\right) \tag{8}$$

Define the equivalent diameter, D_e, as

$$D_e = \frac{4 \text{ (cross section area)}}{\text{wetted perimeter}}$$

$$= 2 (R_1 - R_2) \tag{9}$$

Thus, we have

$$D_e = \frac{2\varepsilon_g{}^p \, d_p}{3\varepsilon_s{}^p} \left[\left(1 + \frac{\varepsilon_\ell{}^p}{\varepsilon_g{}^p}\right) - \sqrt{1 + \frac{\varepsilon_\ell{}^p}{\varepsilon_g{}^p}} \right] \tag{10}$$

Assuming momentum transfer due to acceleration of each phase is negligible, the momentum balance for the liquid and gas phases in the packed bed under steady state conditions can be expressed respectively, by

$$-\left(\frac{dP}{dz}\right)^p = \rho_\ell g + \left(-\frac{dP}{dz}\right)_f^\ell \tag{11}$$

$$-\left(\frac{dP}{dz}\right)^p = \rho_g g + \left(-\frac{dP}{dz}\right)_f^g \tag{12}$$

where $\left(-\frac{dP}{dz}\right)_f^\ell$ is the pressure drop due to friction in the liquid phase which consists of two components; one is contributed by the solid phase or $\left(-\frac{dP}{dz}\right)_f^{\ell-s}$ and the other is contributed by the gas phase of $\left(-\frac{dP}{dz}\right)_f^{\ell-g}$. Mathematically, it can be represented by

$$\left(-\frac{dP}{dz}\right)_f^\ell = \left(-\frac{dP}{dz}\right)_f^{\ell-s} + \left(-\frac{dP}{dz}\right)_f^{\ell-g} \tag{13}$$

The pressure drop due to friction in the gas phase or $(-\frac{dP}{dz})_f^g$ consists of only one component, which is contributed by the liquid phase. Mathematically, it can be represented by

$$(-\frac{dP}{dz})_f^g = (-\frac{dP}{dz})_f^{g-\ell} \tag{14}$$

Since the mutual forces at the interface are cancelled by each other, we have

$$\theta_\ell (-\frac{dP}{dz})_f^{\ell-g} + \theta_g (-\frac{dP}{dz})_f^{g-\ell} = 0 \tag{15}$$

where $\theta_\ell = \frac{\varepsilon_\ell^P}{1-\varepsilon_s^P}$ (16)

$$\theta_g = \frac{\varepsilon_g^P}{1-\varepsilon_s^P} \tag{17}$$

Note that

$$\theta_\ell + \theta_g = 1 \tag{18}$$

From Eqns. (11) through (15), and (18), we obtain

$$(-\frac{dP}{dz})^P = \theta_\ell \rho_\ell g + \theta_g \rho_g g + \theta_\ell (-\frac{dP}{dz})_f^{\ell-s} \tag{19}$$

or

$$(-\frac{dP}{dz})_f^{\ell-s} = \frac{1}{\theta_\ell}[(-\frac{dP}{dz})^P - \theta_\ell \rho_\ell g - \theta_g \rho_g g] \tag{20}$$

Note that $(-\frac{dP}{dz})_f^{\ell-s}$ is negative due to the fact that the liquid flow is downward while z is defined as positive for the upward flow.

The friction factor between the liquid and solid, f, is defined in this work based on Fanning's equation as

$$-(-\frac{dP}{dz})_f^{\ell-s} = 4f(\frac{1}{D_e})(\frac{1}{2}\rho_\ell \overline{U}_\ell^2) \tag{21}$$

$$= 4f(\frac{1}{D_e})[\frac{1}{2}\rho_\ell (\frac{U_{\ell o}}{\varepsilon_\ell^P})^2] \tag{22}$$

The value of f is found to be a function of Re as given in Fig. 4.18. It is seen in the figure that as Re increases, f decreases. f can be empirically correlated as a function of Re by

$$f = 36.94\ Re^{-0.681} \tag{23}$$

where Re is defined as

$$Re = \frac{D_e \rho_\ell \overline{U}_\ell}{\mu_\ell} \tag{24}$$

The agreement between Eqn. (23) and experimental data for f is satisfactory.

Also shown in Fig. 4.18 are the experimental data obtained in this work for the single phase flow involving liquid flow through a packed bed. It is seen that, for the liquid flow in a packed bed, f is well represented by Eqn. (23). A plot of f versus Re based on the Ergun equation is also represented in the figure. It is seen that the data for the liquid flow in a packed bed lie well above the predictions of the Ergun equation at Reynolds numbers below 100.

The gas hold-up in the packed bed is measured by the quick-valve-closing technique. In the present experimental system, a bubble column exists above the packed bed, and thus the total gas volume measured from the liquid level before and after the linked-quick-closing valves are closed requires correction for the gas volume in the bubble column to obtain the true gas volume in the packed bed. The gas volume in the bubble column can readily be obtained from the pressure gradient measurement in the column.

The gas hold-ups in the packed bed, ε_g^p, experimentally obtained are empirically correlated in this study. ε_g^p, which is expressed in terms of

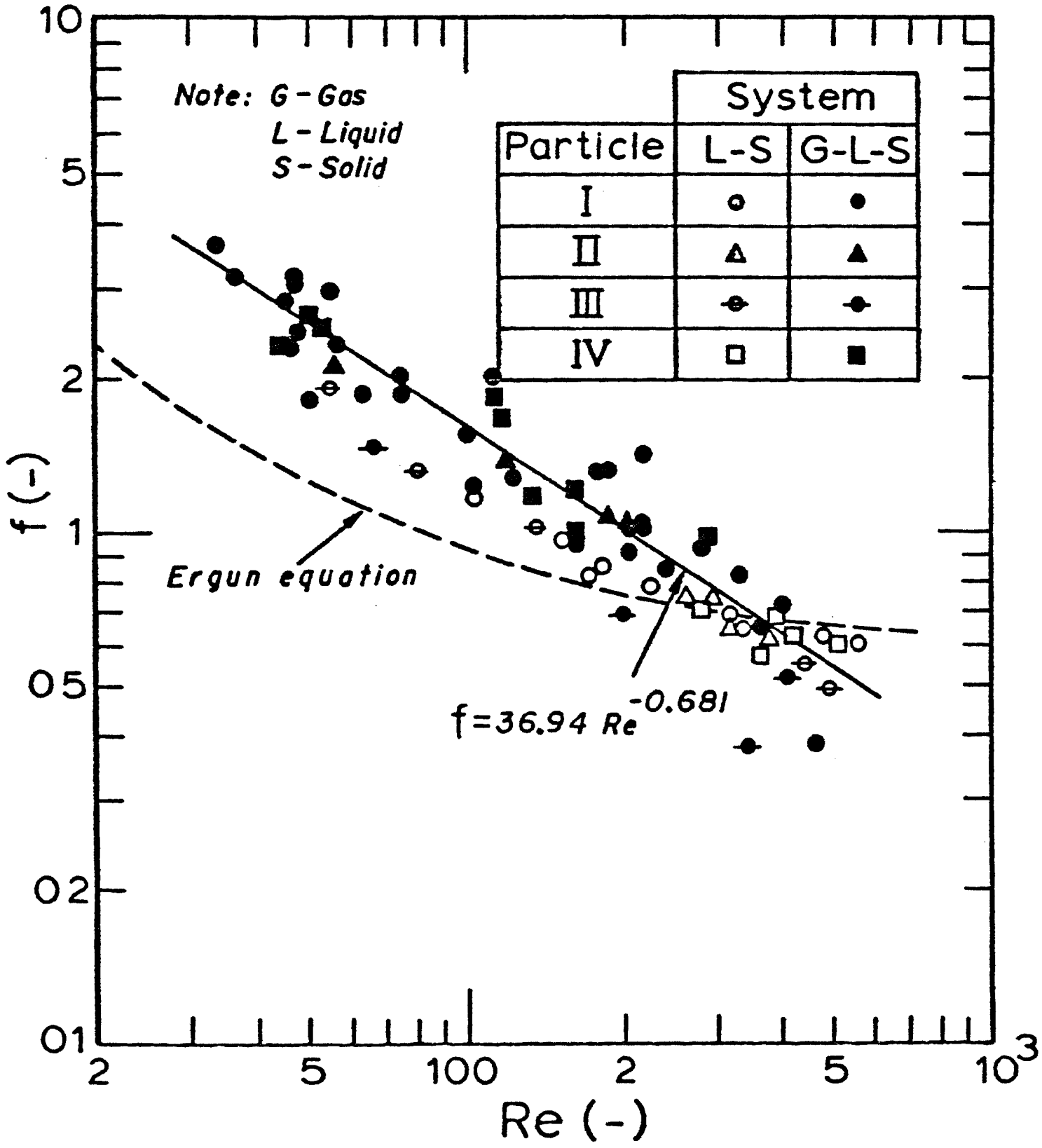

Fig. 4.18. Variation of the Friction Factor f versus Re.

θ_g defined by Eqn. (17) was found to be closely correlated with $U_{\ell o}$ and U_{go} as given by

$$\theta_g = 0.084\ (U_{\ell o})^{0.253}\ (U_{go})^{0.878} \tag{25}$$

The average coefficient of variation for Eqn. (25) is 17.1%.

Based on the equations obtained, a flow diagram is provided in Fig. 4.19 to illustrate the procedures in predicting the pressure gradient in the packed bed. Figure 4.20 shows the comparison between the experimental and calculated values for the pressure gradient. It is seen that the coefficient of variation for 95% of the data is less than 12.1%.

4.2b. CONSTRAINED FLUIDIZED BED AND SEMIFLUIDIZED BED BEHAVIOR

In this experiment, pressure drops in the constrained fluidized bed were measured. Gas hold-ups in the bed were calculated from pressure drop information using the following model equations:

$$(-\Delta p)^f = (\varepsilon_s{}^f \rho_s + \varepsilon_\ell{}^f \rho_\ell + \varepsilon_g{}^f \rho_g)\ H_c g \tag{26}$$

$$\varepsilon_s{}^f = W_s/\rho_s A H_c \tag{27}$$

$$\varepsilon_g{}^f + \varepsilon_\ell{}^f + \varepsilon_s{}^f = 1 \tag{28}$$

Analysis of the gas hold-up and pressure drop in the constrained fluidized bed is given in the following:

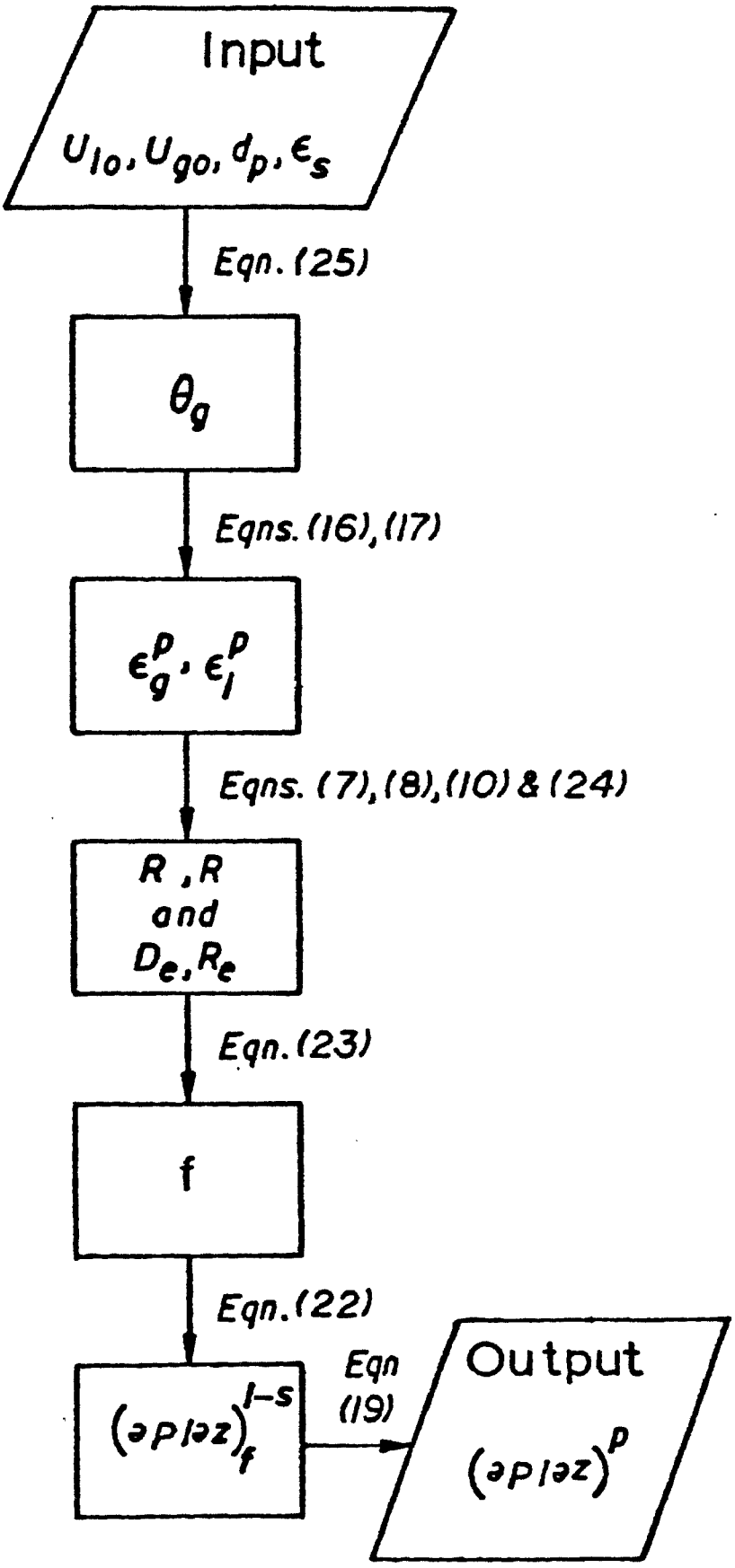

Fig. 4.19. Flow Diagram for Calculation of the Pressure Drop in the Packed Bed.

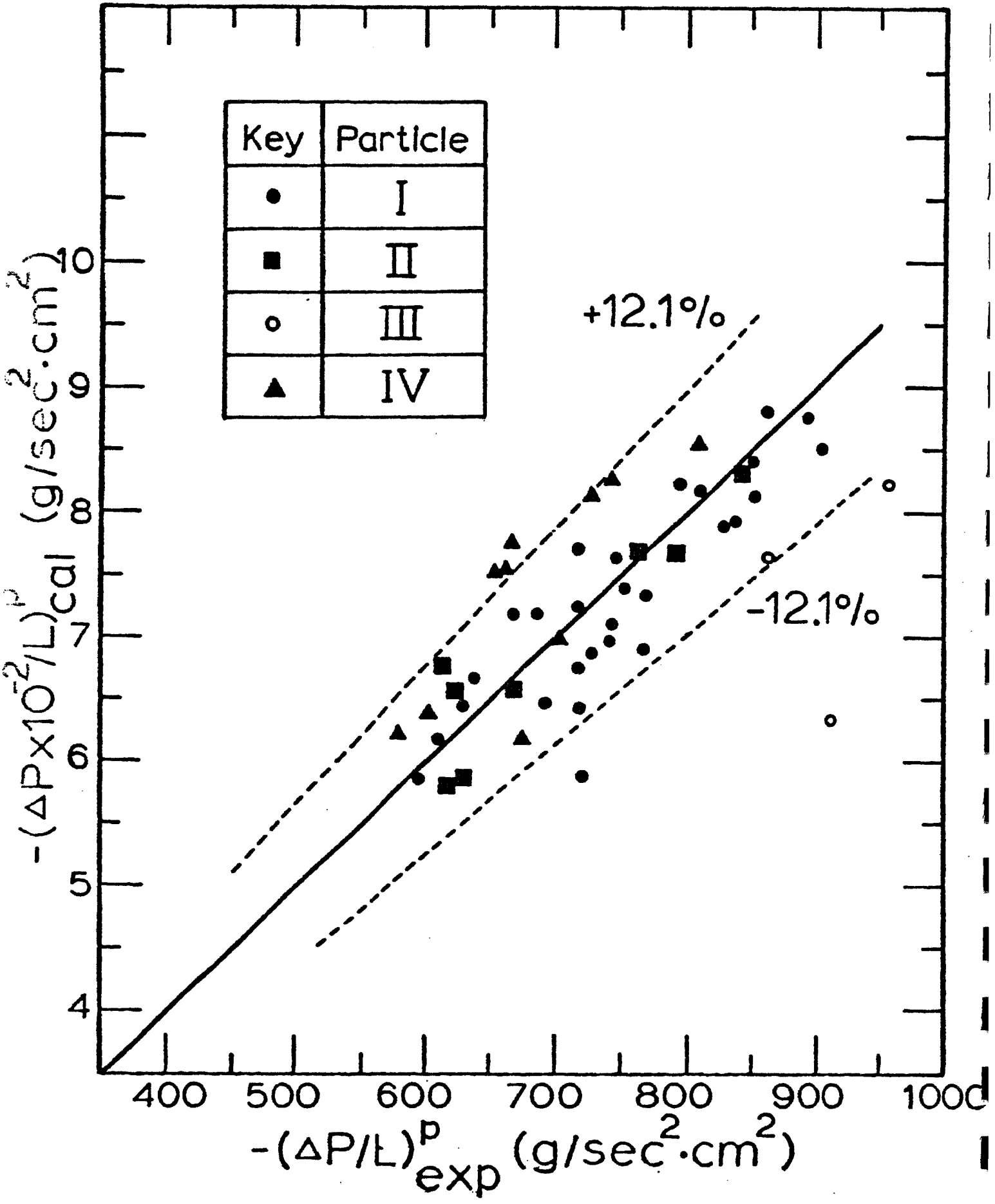

Fig. 4.20. Comparison of the Predicted and Experimental Values for $(-\Delta P/L)^P$ in the Packed Bed.

The gas hold-up in the constrained fluidized bed varies with the solid hold-up, liquid velocity, and gas velocity as shown in Figs. 4.21 and 4.22. In Fig. 4.21, gas hold-up is plotted against gas velocity as a function of liquid velocity while in Fig. 4.22, gas hold-up is plotted against gas velocity as a function of solid hold-up. It is seen that the gas hold-up decreases with increase of the solid hold-up and increase of the liquid velocity. This can be explained in the light of bubble coalescence in the bed. The increase in liquid velocity would increase the particle concentration at the bottom of the bed. As a consequence, bubbles emerging from the gas distributor would undergo coalescence in the environment of low density particles which in turn decreases the gas hold-up in the bed. It is also seen that if the gas velocity is below 4 cm/sec, in which the bed is in the bubbly flow regime, the effects of the solid hold-up and the liquid velocity are more significant than when the gas velocity is above 6 cm/sec, in which the bed is in the slugging flow regime. Wallis' drift flux model is modified here to correlate ε_g^f with $U_{\ell o}$, U_{go}, and ε_s^f as given below:

Define $$J_{gj} = \varepsilon_g^f \, (\bar{U}_g - j) \tag{29}$$

where $$\bar{U}_g = U_{go}/\varepsilon_g^f \tag{30}$$

$$j = U_{go} - U_{\ell o} \tag{31}$$

Note that the expression for j in Eqn. (31) would yield either positive or negative values for j. From Eqns. (28) through (31), we have

$$J_{gj} = \varepsilon_\ell^f \, U_{go} + \varepsilon_g^f \, U_{\ell o} + \varepsilon_s^f \, U_{go} \tag{32}$$

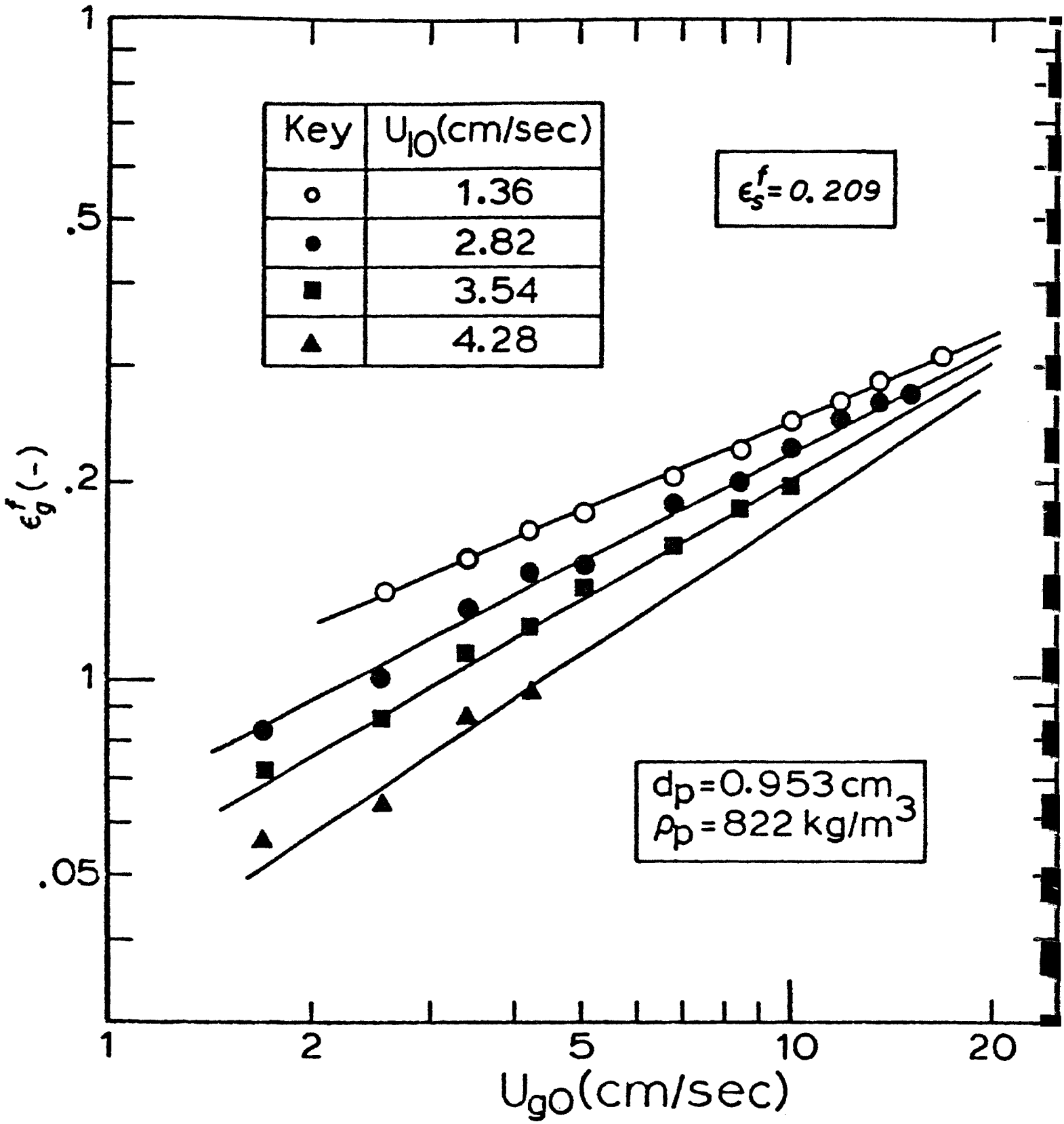

Fig. 4.21 Variation of the Gas Hold-up Versus Gas Velocity as a Function of the Liquid Velocity for the Constrained Inverse Gas-Liquid-Solid Fluidized Bed.

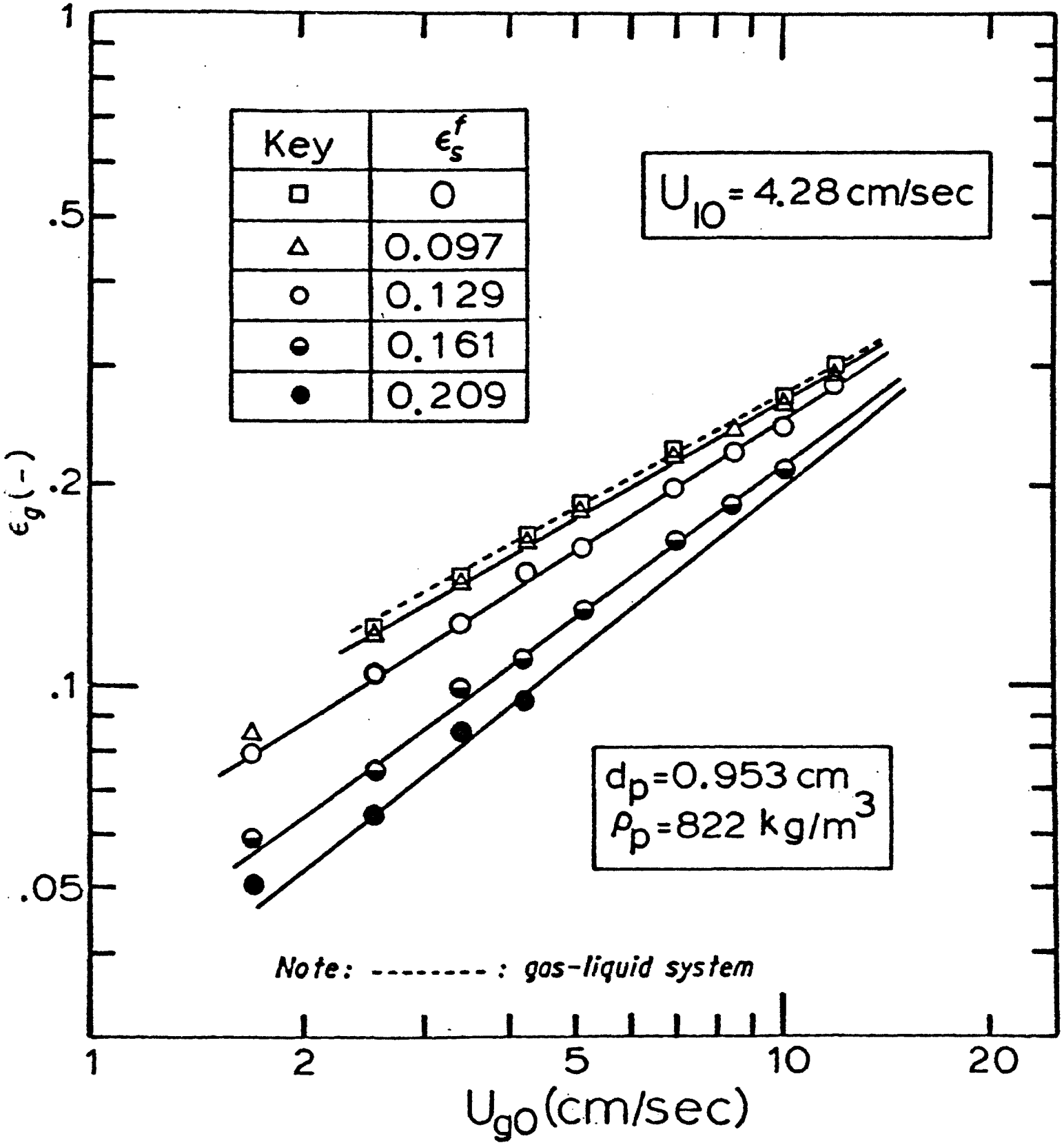

Fig. 4.22. Variation of the Gas Hold-up Versus Gas Velocity as a Function of the Solid Hold-up for the Constrained Inverse Gas-Liquid-Solid Fluidized Bed.

Assume

$$J_{gj} = U_{\infty} \left(\varepsilon_g^f\right)^x \left(1 - \varepsilon_g^f\right)^y \tag{33}$$

where U_{∞} characterizes the single bubble rising velocity in the system which can be expressed as a function of parameters $U_{\ell o}$ and ε_s^f. Thus, an empirical correlation for the dirft flux of gas is proposed in the following to allow the calculation of the gas hold-up:

$$J_{gj} = 32.5 \left(\frac{U_{\ell o}}{U_t}\right)^{0.583} \left(\varepsilon_s^f\right)^{0.583} \left(\varepsilon_g^f\right)^{0.652} \left(1-\varepsilon_g^f\right)^{-4.64} \tag{34}$$

$$\text{for } U_{go} \leq 5.0 \text{ cm/sec.}$$

$$J_{gj} = 102 \left(\frac{U_{\ell o}}{U_t}\right)^{0.191} \left(\varepsilon_s^f\right)^{0.390} \left(\varepsilon_g^f\right)^{1.28} \left(1-\varepsilon_g^f\right)^{-0.440} \tag{35}$$

$$\text{for } U_{go} > 5.0 \text{ cm/sec}$$

U_t in Eqns. (34) and (35) is the extrapolated superficial liquid velocity in a liquid-solid fluidized bed as the bed voidage appraoches 1. The average coefficients of variation of Eqns. (34) and (35) are 8.2% and 9.3%, respectively.

The pressure drop in the constrained fluidized bed is well represented by Eqn. (26). In this equation, ε_s^f can be calculated by Eqn. (27). ε_g^f can be estimated by Eqns. (29), (34), and (35) while ε_ℓ^f can be calculated

by the expression $(1-\varepsilon_g{}^f - \varepsilon_s{}^f)$.

The onset liquid velocity, height of packed section and model and prediction of pressure drop in the constrained semifluidized bed are analyzed in the following:

The formation of the packed bed in the constrained semifluidized bed is a rather complex phenomenon. Prior to the formation of a stable packed bed at the onset of semifluidization, the packed bed is in an unstable state experiencing cyclic destruction by the upward movement of the bubble. Thus, it is difficult to determine the onset liquid velocity for semifluidization solely by visual observation.

In this work, determination of the onset liquid velocity for semifluidization is made based on a plot of the negative of the dynamic pressure drop $-(-\Delta p')$ versus $U_{\ell o}$. An averaged value for the dynamic pressure drop is obtained under the pressure fluctuation conditions. Note that the dynamic pressure drop is the pressure drop corrected for the liquid head, that is

$$(-\Delta p')_d = (-\Delta p') - H_c'\rho_\ell g \tag{36}$$

Under the condition of constrained fluidization, we have

$$\begin{aligned}(-\Delta p')_d &= (\varepsilon_s'\,\rho_s + \varepsilon_\ell'\,\rho_\ell + \varepsilon_g'\,\rho_g)\,H_c'g - H_c'\rho_\ell g \\ &\simeq [\varepsilon_s'\,(\rho_s - \rho_\ell) - \varepsilon_g'\,\rho_\ell]\,H_c'g\end{aligned} \tag{37}$$

where ε_g is the only variable in the right hand side of Eqn. (37).

As described previously, under the condition of constrained fluidization, ε_g' decreases with the increase of $U_{\ell o}$. Thus, noting that ρ_s is smaller than ρ_ℓ, $-(-\Delta p')_d$ would decrease as $U_{\ell o}$ increases prior to the onset of

semifluidization. However, as $U_{\ell o}$ further increases, and a packed bed forms, $-(-\Delta p')_d$ would increase appreciably with $U_{\ell o}$. Thus a break point can be determined from the plot of $-(-\Delta p')_d$ versus $U_{\ell o}$, which defines the onset liquid velocity for semifluidization.

A plot of $-(\Delta p')_d$ versus $U_{\ell o}$ as a function of the gas velocity is shown in Fig. 4.23. The loci of onset semifluidization is also noted in the figure. It is seen that $(U_{\ell o})_{osf}$ decreases as U_{go} increases up to about 5 cm/sec beyond which $(U_{\ell o})_{osf}$ remains nearly constant as U_{go} further increases. Empirical correlations are porposed for $(U_{\ell o})_{osf}$ as follows:

$$(U_{\ell o})_{osf} = 0.0240(Ar)^{0.138}\ (Fr_g)^{-0.0820}(\varepsilon_s')^{-1.50} \qquad (38)$$

The average coefficient of variation of Eqn. (38) is 16.2%.

Empirical correlations for the height of the packed section of the constrained semifluidized bed are proposed as follows:

$$\left(\frac{H_{pa}'}{H_c'}\right) = 66.2\ \ (Ar)^{0.0120}(Fr_\ell)^{0.590}(Fr_g)^{0.0980}(\varepsilon_s')^{3.32} \qquad (39)$$

The average coefficients of variation of Eqn. (39) is 20.5%.

The bubbling behavior in the fluidized section of the constrained semifluidized bed is similar to that of the constrained fluidized bed except that the former has larger inlet bubble size than the latter. The large inlet bubble size in the fluidized section of the constrained semifluidized bed is contributed by the bubble coalescence in the packed section located below the fluidized section. Experimental analysis has been conducted to obtain the gas hold-up in the fluidized section of the constrained semifluidized bed.

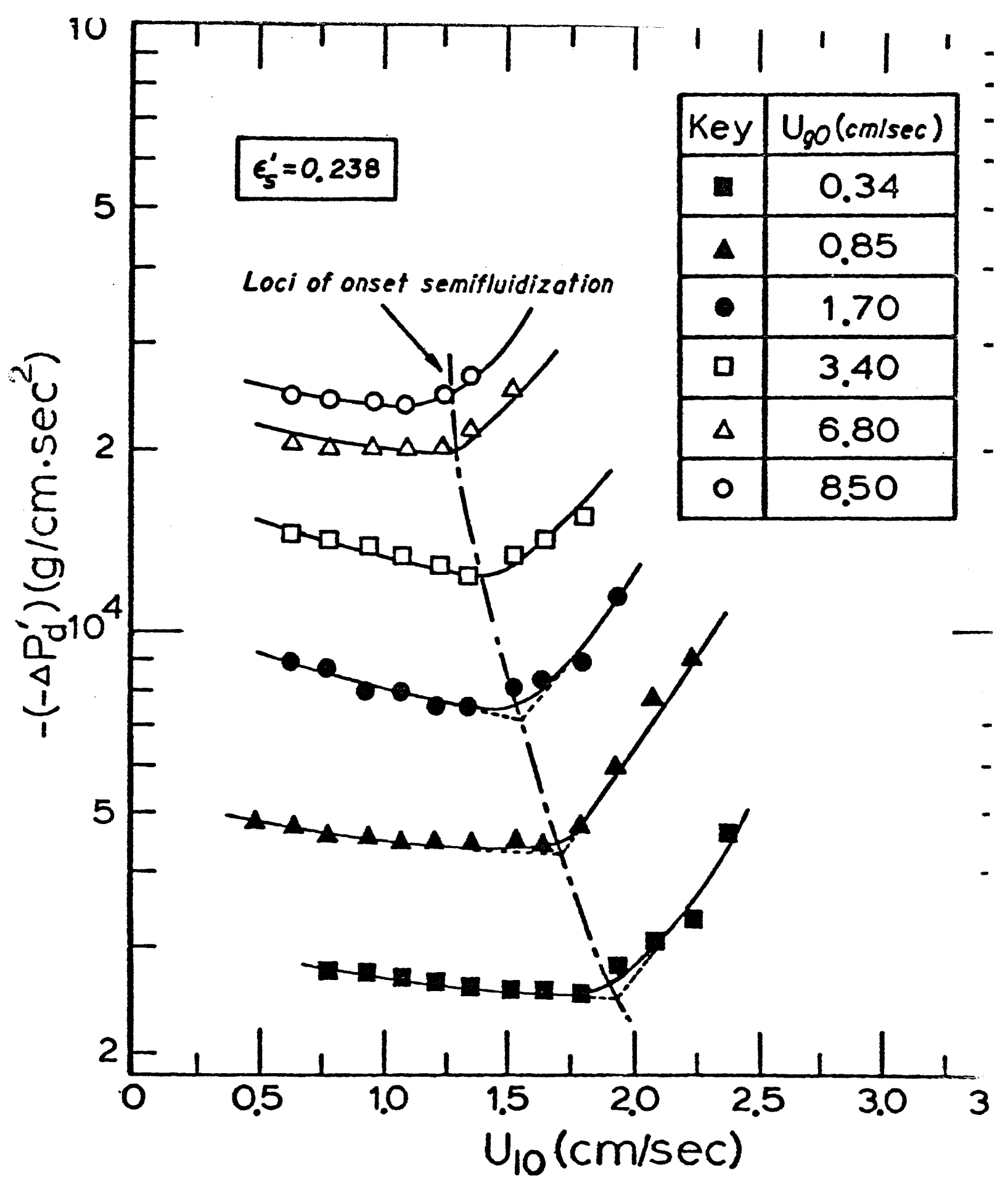

Fig. 4.23. Variation of the Dynamic Pressure Drop Versus the Liquid Velocity During the Transition from Constrained Inverse Fluidization to Constrained Inverse Semifluidization.

It is found that the gas hold-up in the fluidized section $\varepsilon_g'^f$ can be related to that in the constrained fluidized bed, ε_g^f, by the following equation.

$$\varepsilon_g'^f = F \cdot \varepsilon_g^f \tag{40}$$

F in Eqn. (40) is a parameter which is found to vary only with the packed section height, H'_{pa} according to

$$F = \exp(-0.0413\ H'_{pa}) \tag{41}$$

The average coefficient of variation for Eqn. (41) is 33.2%.

The pressure drop in the constrained semifluidized bed is considered to be the sum of the pressure drops in the packed section and the fluidized section, that is,

$$(-\Delta P') = (-\Delta P')^P + (-\Delta P')^f \tag{42}$$

$(-p')^P$, the pressure drop in the packed section, can be readily obtained from the procedures described in Fig. 4.24 with the assumption of

$$1 - \varepsilon_s'^P = \varepsilon_{mf} \tag{43}$$

where ε_{mf} can be estimated by [8]

$$\frac{1}{\phi_s\ \varepsilon_{mf}^3} = 14 \tag{44}$$

with ϕ_s equal to 1 for spherical particles.

The solid hold-up in the fluidized section is readily obtainable from the mass balance equations as given by

$$(H'_c - H'_{pa})\ A\ \varepsilon_s^f + (H'_{pa})\ (A)\ (\varepsilon_s'^P) = (H'_c)\ (A)\ (\varepsilon_s') \tag{45}$$

Thus, we have

$$\varepsilon_s'^f = \frac{H'_c\ \varepsilon_s' - H'_{pa}\ \varepsilon_s'^P}{H_c' - H_{pa}'} \tag{46}$$

The gas hold-up in the fluidized section, $\varepsilon_g'^f$, can be calculated from Eqns. (34), (35), (40) and (41). Note that the solid hold-up which appears in Eqns. (34) and (35) is the solid hold-up in the fluidized section, which is readily obtained from Eqn. (46). Thus, $\varepsilon_\ell'^f$ can be calculated by the expression $(1 - \varepsilon_g'^f - \varepsilon'_s{}^f)$.

With the available information for $\varepsilon_g'^f$, $\varepsilon_s'^f$, $\varepsilon_\ell'^f$, and H_c', the pressure drop in the fluidized section can be obtained by Eqn. (26).

The flow diagram which describes the computational procedures required to estimate the pressure drop in the constrained semifluidized bed is given in Fig. 4.24. The comparison between the predicted and experimental values of the pressure drop in the constrained semifluidized bed is shown in Fig. 3.25. It is seen that the agreement is good.

Note that in Fig. 3.12, there is no adjustable parameter involved in the correlation equations for prediction of the pressure drop in the constrained semifluidized bed.

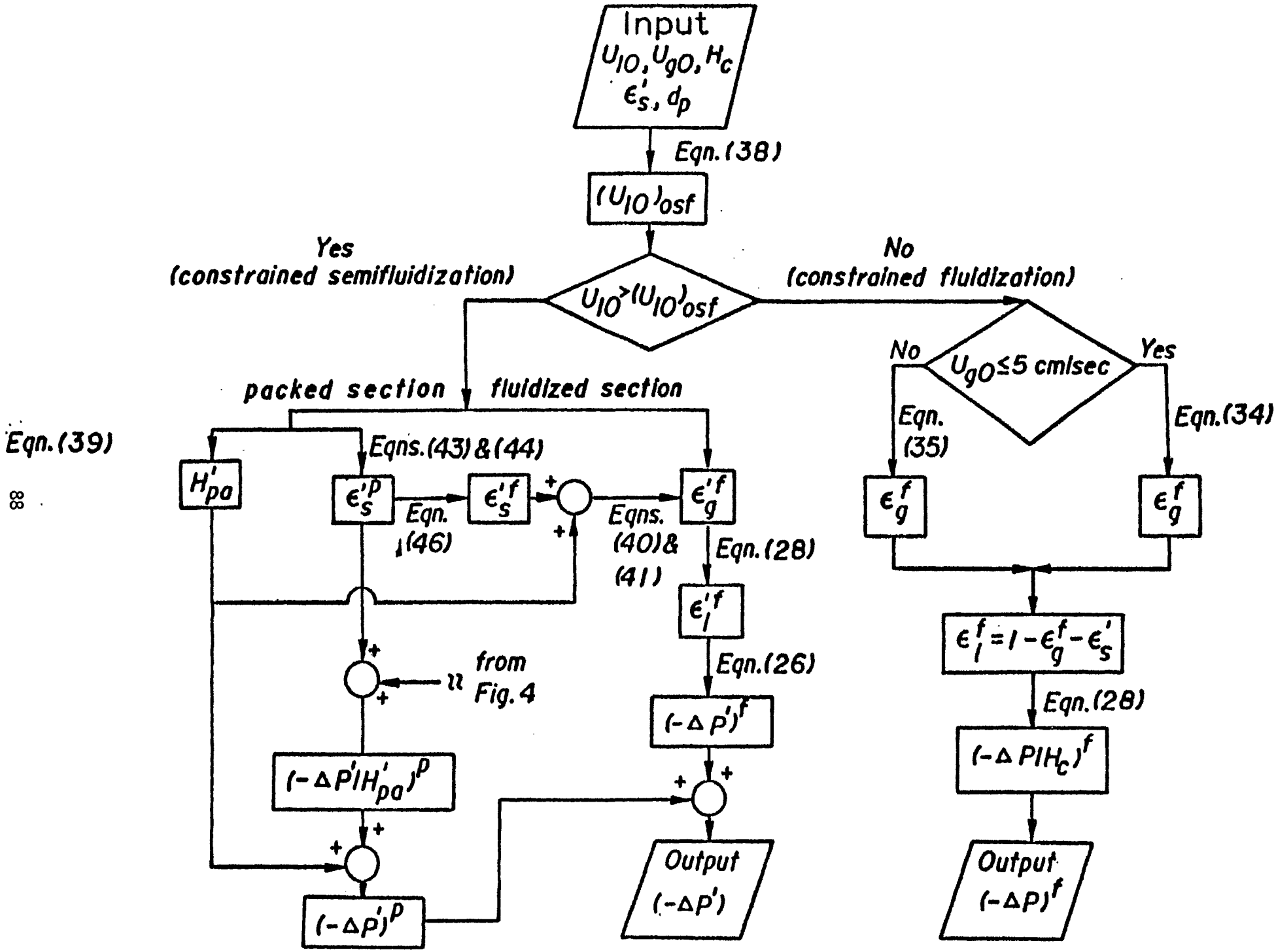

Figure 4.24 Flow Diagram for Calculation of the Pressure Drop in the Constrained Fluidized Bed

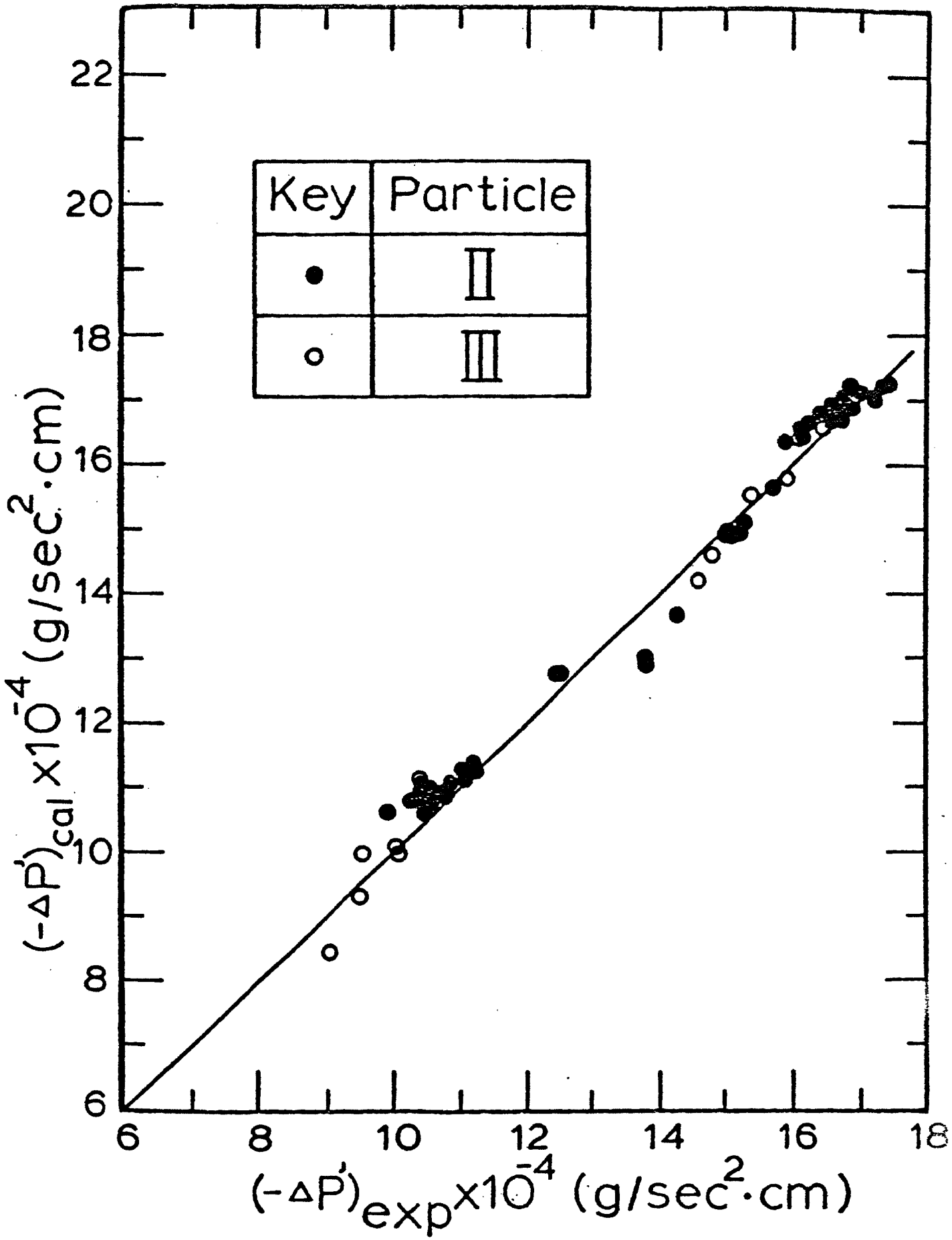

Fig. 4.25. Comparison of the Predicted and Experimental Values for $(-\Delta P')$ in the Constrained INverse Semifluidized Bed.

V. CONCLUSIONS

A. Biological Study

1. Sewage bacteria can be effectively acclimated for phenol degradation.
2. The effect of temperature on phenol degradation rates at phenol concentrations of 200 mg/L or less is insignificant.
3. The inhibiting effect of high phenol concentration appears to be temperature dependent. The optimum operating temperature is dependent on the phenol concentration.
4. A rule-of-thumb operating temperature for varying concentrations of phenol is 35°C.
5. Phenol degradation is increased by increasing the retention time of the liquid waste in the reactor.
6. The bacteria appear to adhere better to the polypropylene packing than to the charcoal or polyethylene packing.
7. Increased air flowrates caused a slight increase in phenol degradation. However, due to the low amount of phenol degraded, conclusive evidence on the effect of air flowrate on phenol degradation was not possible.
8. A retention time of approximately 75 minutes would be necessary to degrade 50 mg/L of phenol in a packed bed with a surface area of approximately 5.74 ft^2.

B. Hydrodynamics Study

1. The friction factor defined in this study for countercurrent flow of gas and liquid in the packed bed with the liquid as the continuous phase can be empirically correlated by Eqn. (24).

2. Wallis' drift flux model expressed by Eqns. (34) and (35) can be used to determine the gas hold-up in the constrained fluidized bed.
3. The onset liquid velocity for semifluidization can be determined based on the relationship between the dynamic pressure drop and the superficial liquid velocity. The onset liquid velocity for semifluidization can be related to Ar, Fr_g and ε_s' according to Eqn. (38). Equations (34), (35), (40) and (41) can be employed to accurately predict the gas hold-up for the fluidized section while Eqn. (39) can be utilized to account for the height of the packed section in the constrained semifluidized bed.
4. The pressure drop in the constrained inverse semifluidized bed can be represented by the sum of that in the fluidized section and that in the packed section. A computational procedure is developed which allows accurate prediction of pressure drop in the constrained semifluidized bed.

NOMENCLATURE

A	cross-section area of testing column, cm^2
Ar	Archimedes number, defined as $\frac{d_p^3(\rho_\ell-\rho_s)\rho_\ell g}{\mu_\ell^2}$
D	diameter of testing column, cm
d_p	diameter of particle, cm
D_e	equivalent diameter, defined by Eqn. (10), cm
f	modified friction factor, defined by Eqn. (23), -
Fr_ℓ	Froude number for liquid, defined as $\frac{U_{\ell o}^2}{d_p g}$,
Fr_g	Froude number for gas, defined as $\frac{U_{go}^2}{d_p g}$
g	gravitational acceleration, cm/sec^2
H_c	height of testing column, cm
H_{pa}	height of packed bed, cm
J_{gj}	drift flux of gas, defined by Eqn. (29), cm/sec
L_e	equivalent length, shown in Fig. 2, cm
$(-\frac{dP}{dz})$	static pressure gradient, $g/sec^2 \cdot cm^2$
$(-\Delta p)$	static pressure drop, $g/sec^2 \cdot cm$
R_1, R_2	radius, shown in Fig. 2, cm
Re	modified Reynolds number, defined by Eqn. (24)
$\overline{U}$	linear velocity, cm/sec
U_{go}	superficial gas velocity, cm/sec
$U_{\ell o}$	superficial liquid velocity, cm/sec
U_t	extrapolated superficial liquid velocity in a liquid-solid fluidized bed as bed voidage approaches 1.
U_∞	parameter defined in Eqn. (33), cm/sec

Greek Letters

ε	hold-up, -
ε_{mf}	bed voidage at the minimum fluidization condition, -
ϕ_s	shape factor, -
θ	hold-up based on the gas and liquid phases, -
ρ	density, g/cm^3

Superscript

'	semifluidized bed
p	packed bed
f	fluidized bed
ℓ-s	liquid-solid
ℓ-g	liquid-gas
g-ℓ	gas-liquid

Subscript

cal	calculated
f	friction
d	dynamic
exp	experimental
g	gas phase
ℓ	liquid phase
s	solid phase

References

1. Babu Rao, K. and Doraiswamy, L. K. (1970) Combined Reactors: Formulation of Criteria and Operation of a Mixed Tubular Semi-fluidized Reactor. A.I.Ch.E. J. 16 (2), 273.

2. Bayly, R. C. and Dagley, S. (1969) Oxoenoic Acids as Metabolites in the Bacterial Degradation of Catechols. Biochem. J. III, 303.

3. Bayly, R. C., Dagley, S. and Gibson, D. T. (1966) The Metabolism of Cresols by Species of Pseudomonas, Biochem. J. 101, 293.

4. Bennett, C. O. and Myers, J. E. (1974) Momentum, Heat, and Mass Transfer, Second Edition. McGraw-Hill, New York.

5. Breed, R. S., Murray, E. G. D., and Smith, N. R. (1964) Bergey's Manual of Determinative Bacteriology, Williams and Wilkins Co., Baltimore, Md.

6. Brink, Jr., J. A. and Shreve, R. N. (1977) Chemical Process Industries, Fourth Edition. McGraw-Hill, New York.

7. Callely, A. G. (1978) The Microbial Degradation of Heterocyclic Compounds. Progress in Industrial Microbiology, Vol. 14, M. J. Bull, editor, Elsevier Scientific Publishing Co., New York.

8. Chementator (1962), Japanese Report Large-Scale Use of Continuous Ion Exchange. Chem. Eng. 69 (24), 50.

9. Chementator (1972), Fluidized-bed Ion-exchange Systems Are Available. Chem. Eng. 79 (16), 75.

10. Dagley, S. (1971). Catabolism of Aromatic Compounds by Micro-Organisms. Advances in Microbial Physiology Vol. 6, A. M. Rose and J. R. Wilkinson, editors, Academic Press, New York.

11. Dagley, S., Evans, N. C., and Ribbons, D. W. (1960) New Pathways in the Oxidative Metabolism of Aromatic Compounds by Micro-Organisms. Nature 188, 560.

12. Dagley, S. and Gibson, D. T. (1965) The Bacterial Degradation of Catechol. Biochem. J. 95, 466.

13. Dagley, S. and Stopher, B. A. (1959) A New Mode of Fission of the Benzene Nucleus by Bacteria. Biochem. J. 73, 16P.

14. Dann, H. C., Resch, F. K., and Goldwyn, A. J., editors (1968) The Handbook of Biochemistry and Biophysics. World Publishing Co., Cleveland, Ohio.

15. Elvidge, J. A., Linstead, R. P., Sims, P., and Orkin, R. A. (1950) The Third Isomeric (cis-trans-) Muconic Acid. J. Chem. Soc., 2235.

16. Evans, W. C. (1947) Oxidation of Phenol and Benzoic Acid by Some Soil Bacteria. Biochem. J. 41, 373.

17. Evans, W. C., Linstead, R. P., Smith, B. S. W., and Elvidge, J. A. (1951) Chemistry of the Oxidative Metabolism of Certain Aromatic Compounds by Micro-Organisms. Nature 168, 772.

18. Evans, W. C. and Smith, B. S. W. (1951) The Oxidation of Aromatic Compounds by Soil Bacteria. Biochem. J. 49, X.

19. Fan, L. S. (1979) Semifluidized Beds as Bioreactors for Treatment of Waste Liquors from Coal Processing. Proposal to Mining and Mineral Institute, The Ohio State University, Columbus, Ohio.

20. Fan, L. T. and Wen, C. Y. (1961) Mechanisms of Semifluidization of Single Size Particles in Solid-Liquid System. A.I.Ch.E. Journal 7, 606.

21. Fan, L. T., Yang, Y. C., and Wen, C. Y. (1959) Semifluidization: Mass Transfer in Semifluidized Beds. A.I.Ch.E. Journal 5, 407.

22. Fan, L. T., Yang, Y. C., and Wen, C. Y. (1960) Mass Transfer in Semifluidized Beds for Solid-Liquid System. A.I.Ch.E. Journal 6, 482.

23. Farr, D. R. and Cain, R. B. (1968) Catechol Oxygenase Induction in Pseudomonas aeruginosa. Biochem. J. 106, 879.

24. Greenberg, D. J., editor (1969) Metabolic Pathways, Vol. 3. Academic Press, New York.

25. Happold, F. C. (1930) The Correlation of the Oxidation of Certain Phenols and of Dimethyl-p-Phenylenediamine by Bacterial Suspensions. Biochem. J. 24, 1737.

26. Haug, R. T. and McCarty, P. L. (1972) Nitrification with the Submerged Filter. Journal Water Pollution Control Federation 44, 2086.

27. Hawk, P. B. and Oser, B. L., Summerson, W. H. (1954) Practical Physiological Chemistry. Blakiston Co., Inc., New York.

28. Hayaishi, O. and Hashimoto, Z. (1950 Med. J. Osaka University 2, 33.

29. Hayaishi, O., Katagiri, M., and Rothberg, S. (1957) Mechanism of the Pyrocatechase Reaction. J. Am. Chem. Soc. 77, 5450.

30. Hayaishi, O., Katagiri, M., and Rothberg, S. (1957) Studies on Oxygenases. J. Biol. Chem. 229, 905.

31. Haynes, W. P. and Forney, A. J. (1975) High Btu Gas from Coal: Status and Prospects. Pittsburg Energy Research Center, Energy Research and Development Administration.

32. Holladay, D. W., Chilcote, D. D., Hancher, C. W., and Scott, C. D. (1978) Biodegradation of Phenolic Waste Liquors in Stirred-Tank, Packed-Bed, and Fluidized-Bed Bioreactors. Journal Water Pollution Control Federation 50, 2573.

33. Jeris, J. S. and Owens, R. W. (1975) Pilot-Scale High-Rate Biological Denitrification. Journal Water Pollution Control Federation 47, 2043.

34. Jeris, J. S., Beer, C., and Mueller, J. A. (1974) High rate Biological Denitrification Using a Granular Fluidized Bed. Journal Water Pollution Control Federation 46, 2118.

35. Johnson, R. L., and Baumann, E. R. (1971) Advanced Organic Removal by Pulsed Adsorption Beds. Journal Water Pollution Control Federation 43, 1640.

36. Katagiri, M. and Hayaishi, O. (1957) Enzymatic Degradation of β-ketoadipic Acid. J. Biol. Chem. 226, 439.

37. Kilby, B. A. (1948) The Bacterial Oxidation of Phenol to β-ketoadipic Acid. Biochem. J. 43, V.

38. Kilby, B. A. (1951) The Formation of β-ketoadipic Acid by Bacterial Fission of Aromatic Rings. Biochem. J. 49, 671.

39. Kojima, Y., Itada, N. and Hayaishi, O. (1961) Metapyrocatechase: A New Catechol-cleaving Enzyme. J. Biol. Chem. 236, 2223.

40. Lee, D. D., Scott, C. D., and Hancher, C. W. (1979) Fluidized bed Bioreactor for Coal Conversion Effluents. Journal Water Pollution Control Federation 51, 974.

41. Nakazawa, T., Kojima, Y., Fujisawa, H., Nozaka, M., and Hayaishi, O. (1965) Studies on the Mechanism of Action of Pyrocatechase by Electron Spin Resonance Spectroscopy. J. Biol. Chem. 240, PC 3224.

42. Nishizuka, Y., Ichiyama, A., Nakamura, S., and Hayaishi, O. (1962) A New Metabolic Pathway of Catechol. J. Biol. Chem. 237, PC268.

43. Ornston, L. N. (1966) The Conversion of Catechol and Protocatechuate to β-ketoadipate by Pseudomonas putida. J. Biol. Chem. 241, 3800.

44. Ornston, L. N. and Stanier, R. Y. (1966) The Conversion of Catechol and Protocatechuate to β-ketoadipate by Pseudomonas putida, Part I. Biochemistry. J. Biol. Chem. 241, 3776.

45. Overman, A. R., Chu, R. L., and Leseman, W. G. (1976) Phosphorous Transport in a Packed Bed Reactor. Journal Water Pollution Control Federation 48, 880.

46. Overman, A. R., Chu, Ro-Lan, and Le, Y. (1978) Kinetic Coefficients for Phosphorous Transport in Packed-Bed Reactor. Journal Water Pollution Control Federation 50, 1905.

47. Pitea, D., Beltrame, P., Beltrame, P. L. and Carniti, P. (1980) Kinectics of Phenol Degradation by Activated Sludge in a Continuous-Stirred Reactor. Journal Water Pollution Control Federation 52, 126.

48. Pitt, Jr., W. W., Hancer, C. W., and Hsu, H. W. (1978) The Tapered Fluidized Bed Bioreactor--An Improved Device for Continuous Cultivation. A.I.Ch.E. Symposium Series, 74, 119.

49. Requa, D. A. and Schroeder, E. D. (1973) Kinetics of Packed-Bed Denitrification. Journal Water Pollution Control Federation 45, 1697.

50. Scott, C. D. and Hancher, C. W. (1976) Use of a Tapered Fluidized Bed as a Continuous Bioreactor. Biotechnology and Bioengineering 18, 1393.

51. Skidmore, D. R., Fong, F. K., Sykes, R. M., Stiefel, R. C., Bailey, R. E., and Herdendorf, P. B. (1979) Wastewater Production and Treatment for Synethetic Fuel Processes in the Ohio River Basin. The Ohio River Basin Commission, Water Resources Center, The Ohio State University, Columbus, Ohio.

52. Standard Methods for the Examination of Water and Wastewater, Thirteenth Edition (1971) Amer. Pub. Health Assn., Washington, D.C. (1971).

53. Stanier, R. Y. (1968) Control of the Enzymes of the β-Oxoadipate Pathway in Bacteria. Biochem. J. 106, 25P.

54. Stanier, R. Y., Sleeper, B. P., Tsuchida, M., and McDonald, D. L. (1950) The Bacterial Oxidation of Aromatic Compounds. J. Bact. 59, 137.

55. Stevenson, L. L. and Mandelstan, J. (1965) Induction and Multi-Sensitive End Product Repression in Two Converging Pathways Degrading Aromatic Substances in Pseudomonas fluorescens. Biochem. J. 96, 354.

56. Vereecken, J. and Borighem, G. (1978) Study of the Biodegradation of Phenol in River Water. Biological Modelling 4, 51.

57. Wastewater Treatment Unit Features Fluidized Bed (1976). Chem. Eng. 83, 87. (October 25, 1976)

58. Weber, Jr., W. J. and Ying, W. C. (1978) Biophysicochemical Adsorption Systems for Wastewater Treatment: Predictive Modeling for Design and Operation. Proc. 33rd Ind. Waste Conf., Purdue University, W. Lafayette, Ind.

59. Weiser, H. H., Randles, C. I., Sherrer, E. L., and Hamdy, M. K. (1955) Some Characteristics of a Phenol-Oxidizing Pseudomonas. The Engineering Experiment Station, The Ohio State University Bulletin No. 157.

60. Wen, C. Y., Wang, S. C., and Fan, L. T. (1963) Semifluidization in Solid-Gas Systems. A.I.Ch.E. Journal 9, 316.

61. Yang, R. D. and Humphrey, A. E. (1975) Dynamic and Steady State Studies of Phenol Biodegradation in Pure and Mixed Cultures, Biotechnology and Bioengineering 17, 1211.

62. Young, J. C., Baumann, E. R., and Wall, D. J. (1975) Packed-Bed Reactors for Secondary Effluent BOD and Ammonia Removal. Journal Water Pollution Control Federation 47, 46.

63. Young, J. C. and McCarty, P. L. (1969) The Anaerobic Filter for Waste Treatment. Journal Water Pollution Control Federation 41, R160.

APPENDIX

Laboratory Analysis of Bacteria

LABORATORY REPORT

REPORT TO:

Chemical Engineering Dept.
Attn: Anne Edwards
Ohio State University
140 W. 19th
Columbus, OH 43210

analysis for:	sample no.
Anne Edwards/Chem. Engin	5037
address: Koffolt Labs/ Ohio State University	
product description: Bacterial suspenion in synthetic broth	received: Oct 6 analyzed: Oct 6-30 reported: Nov 4, 1980

ISOLATE	REACTIONS																		
	GRAM REACTION	MORPHOLOGY	OXIDASE	CATALASE	MOTILITY	PIGMENTED COLONY	McCONKEYS GROWTH?	GROWTH ON TSI?	VOGES-PROSKAUER	NITRATE REDUCTASE	PHENYLALANINE RXN	HYDROGEN SULFIDE	INDOLE	UREASE	B-GALACTOSIDASE	ARABINOSE FERM.	SORBITOL FERM.	INOSITOL FERM
1. Pseudomonas putida	G-	rod	+	-	+/-	neg	+	a[3]a[3]-[3]	-	+	+	-	-	+	+	+	-	-
2. Providencae alcalifaciens	G-	rod	-	+	-	neg	+	aa-	-	-	+	-	+	-	-	-	+	-
3. Citrobacter freundiae	G-	rod	-	+	-	1	+	Aa-	-	+	+/-	+	-	-	-	+	+	-
4. Proteus (mirabilis?)	G-	rod	-	+	+/-	neg	+	A[3]a-	-	+	-	-	+	-	-	-	-	-
5. Flavobacter	G-	rod	-	-	-	2	+	aa-	-	-	-	-	+	-	-	-	-	-

Notes: 1 ... *light orange colonies*
2 ... *yellow colonies*
[3] ... *1st letter: pH reaction on slant of tube*
2nd letter: pH reaction in butt of tube
3rd symbol: presence or absence of gas production
3 ... "a" = *alkaline reaction @ 24 hrs.*
"A" = *acid reaction @ 24 hrs.*
"-" = *no gas production.*
"+" = *positive for gas.*

ANALYST

LYLE LABORATORIES 1500 W THIRD COLUMBUS, OHIO 43212